Mineralogy and Petrology

On the origin of mafic magmatic enclaves (MMEs) in the syncollisional granitoids: Evidence from the Baojishan pluton in the North Qilian Orogen, China

--Manuscript Draft--

Manuscript Number:	MIPE-D-14-00098R2
Full Title:	On the origin of mafic magmatic enclaves (MMEs) in the syncollisional granitoids: Evidence from the Baojishan pluton in the North Qilian Orogen, China
Article Type:	Standard Article
Keywords:	Keywords: Mafic magmatic enclaves; cumulate origin; syn-collisional granodiorite; North Qilian Orogen
Corresponding Author:	shuo chen Institute of Oceanology, Chinese Academy of Sciences qingdao, CHINA
Corresponding Author Secondary Information:	
Corresponding Author's Institution:	Institute of Oceanology, Chinese Academy of Sciences
Corresponding Author's Secondary Institution:	
First Author:	shuo chen
First Author Secondary Information:	
Order of Authors:	shuo chen
	Yaoling Niu
	Wenli Sun
	Yu Zhang
	Jiyong Li
	Pengyuan Guo
	Pu Sun
Order of Authors Secondary Information:	
Funding Information:	geological survey projects of China Geological Survey Departments and Offices (1212011121092) — Yaoling Niu
	geological survey projects of China Geological Survey Departments and Offices (1212011220928) — Yaoling Niu
	National Natural Science Foundation of China (91014003) — Yaoling Niu
	National Natural Science Foundation of China (41130314) — Yaoling Niu
Abstract:	Mafic magmatic enclaves (MMEs) are abundant in Baojishan syn-collisional granitoids located in the eastern section of the North Qilian Orogen. Zircon U-Pb ages of the host granodiorite (433.7±3.4 Ma) and their MMEs (431.6±2.8 Ma) are the same as the time of the Qilian Ocean closing and continental collision at ~440 - 420Ma, indicating that the granitoids represent a magmatic response to the collision between the Qilian-Qaidam block and the Alashan block. The MMEs have the same mineralogy as the host granodiorite except that they are more abundant in mafic phases (e.g., amphibole and biotite) and thus have higher heavy rare earth element (HREE) abundances. Both the host granodiorite and the MMEs have light REE-enriched patterns and relatively flat

	HREE patterns (i.e., [Dy/Yb]N =1 - 1.1). They are enriched in large ion lithophile elements (LILEs; e.g., Rb, K, Pb) and depleted in high field strength elements (HFSEs; e.g., Nb, Ta, Ti) and show a varying Sr anomaly (i.e., Sr/Sr* = 0.9 - 2.2) for the host and a negative Sr anomaly (i.e., Sr/Sr* = 0.4 - 0.6) for the MMEs. Both the host granodiorite and the MMEs have overlapping and indistinguishable Sr-Nd-Hf isotopic compositions (87Sr/86Sr(i)=0.7067 - 0.7082, εNd(t) =-3.9 - -3.2, εHf(t)=1.0 - 14.7). The extremely high εHf(t)=14.7 of sample BJS12-06MME likely results from the calculation due to nugget effect of zircons because of the unexpectedly high Hf (3.53 ppm) and too high Zr (128 ppm). All these characteristics are fully consistent with the MMEs being of cumulate origin formed at earlier stages of the same magmatic systems rather than representing mantle melt required by the popular and alleged magma mixing model. The radiogenic Sr and unradiogenic Nd (εNd(t) <0) indicate the contribution of mature continental crust, while variably radiogenic Hf (εHf(t) > 0) for both the MMEs and their host granodiorite manifest the significant mantle input. The apparent decoupling between Nd and Hf isotopes are likely caused by partial melting of recycled terrigenous sediments and the remaining part of the North Qilian ocean crust under the amphibolite facies conditions during the collision.
Response to Reviewers:	Thank you very much for your handling of our revised manuscript (ID: MIPE-D-14-00098R1). Following your kind advice, we checked our EMPA data carefully, and have redone the EPMA analyses immediately after having re-polished our thin sections. Though the data (revise Table 2 and Table 3) are similar to previous ones and the interpretation is thus rational. We apologize for our EPMA data with low totals.

On the origin of mafic magmatic enclaves (MMEs) in syn-collisional granitoids: evidence from the Baojishan pluton in the North Qilian Orogen, China

Shuo Chen [a*], Yaoling Niu[a, b*], Wenli Sun[c], Yu Zhang [c], Jiyong Li[a], Pengyuan Guo[c], Pu Sun[a]

[a] Institute of Oceanology, Chinese Academy of Sciences, Qingdao 266071, China.

[b] Department of Earth Sciences, Durham University, Durham DH1 3LE, UK

[c] School of Earth Sciences, Lanzhou University, Lanzhou 730000, China

Abstract: 311 words; text: 8168 words; Table: 6; Figure: 12; Appendices:

***Corresponding author:**

Mr. Shuo Chen (chenshuo528@foxmail.com)

Professor Yaoling Niu (yaoling.niu@foxmail.com)

Current address: Institute of Oceanology

Chinese Academy of Sciences

7 Nanhai Road, Qingdao, Shandong 266071, China

Phone and Fax: +86 0532 8289980

Abstract

Mafic magmatic enclaves (MMEs) are abundant in Baojishan syn-collisional granitoids located in the eastern section of the North Qilian Orogen. Zircon U-Pb ages of the host granodiorite (433.7±3.4 Ma) and their MMEs (431.6±2.8 Ma) are the same as the time of the Qilian ocean closing and continental collision at ~440 - 420Ma, indicating that the granitoids represent a magmatic response to the collision between the Qilian-Qaidam block and the Alashan block. The MMEs have the same mineralogy as the host granodiorite except that they are more abundant in mafic phases (e.g., amphibole and biotite) and thus have higher heavy rare earth element (HREE) abundances. Both the host granodiorite and the MMEs have light REE-enriched patterns and relatively flat HREE patterns (i.e., $[Dy/Yb]_N$ =1 - 1.1)**.** They are enriched in large ion lithophile elements (LILEs; e.g., Rb, K, Pb) and depleted in high field strength elements (HFSEs; e.g., Nb, Ta, Ti) and show a varying Sr anomaly (i.e., Sr/Sr* = 0.9 - 2.2) for the host and a negative Sr anomaly (i.e., Sr/Sr* = 0.4 - 0.6) for the MMEs. Both the host granodiorite and the MMEs have overlapping and indistinguishable Sr-Nd-Hf isotopic compositions ($^{87}Sr/^{86}Sr_{(i)}$=0.7067 - 0.7082, $\varepsilon_{Nd}(t)$ =-3.9 - -3.2, $\varepsilon_{Hf}(t)$=1.0 - 14.7). The extremely high $\varepsilon_{Hf}(t)$=14.7 of sample BJS12-06MME likely results from the calculation due to nugget effect of zircons because of the unexpectedly high Hf (3.53 ppm) and too high Zr (128 ppm). All these characteristics are fully consistent with the MMEs being of cumulate origin formed at earlier stages of the same magmatic systems rather than representing mantle melt required by the popular and alleged magma mixing model. The radiogenic Sr and unradiogenic Nd ($\varepsilon_{Nd}(t)$ <0) indicate the contribution of mature continental crust, while variably radiogenic Hf ($\varepsilon_{Hf}(t)$ > 0) for both the MMEs and their host granodiorite manifest the significant mantle input. The apparent decoupling between Nd and Hf isotopes are likely caused by partial melting of recycled terrigenous sediments and the remaining part of the North Qilian ocean crust under the amphibolite facies conditions during the collision.

Keywords: Mafic magmatic enclaves; cumulate origin; syn-collisional granodiorite; North Qilian Orogen

1 Introduction

Mafic magmatic enclaves (MMEs) are common in calc-alkaline granitoids and are considered as offering key information towards understanding the petrogenesis of such granitoids (Didier 1973; Barbarin and Didier 1991). Detailed field and petrographic features of MMEs have been documented by many investigators since the descriptive work by Phillips (1880). When studying the Sierra Nevada batholith, Pabst (1928) described the MMEs as "autoliths", meaning that the MMEs may be "cogenetic" or part of the same system. Based on geochemical data, Dodge and Kistler (1990) confirmed Pabst's (1928) "autoliths" hypothesis and further proposed that MMEs in central Sierra Nevada were formed from the enclosing magma by early crystallization/accumulation of plagioclase, hornblende and biotite etc. Studies over the years (e.g., Vernon 1983; Didier 1987; Dorais et al. 1990; Castro et al.1990; Barbarin and Didier 1991; Barbarin 2005; Chen et al. 2009a 2009b, 2013; Ma et al. 2013) have recognized the possible relationship of MMEs with some mafic dikes in time and space, which have led to the proposal of a genetic link between them (see Barbarin 2005) although this view ignores the "autoliths" nature of the MMEs with the host (see Niu et al. 2013). As a result, MMEs have been popularly interpreted as evidence of magma mixing between mantle derived basaltic melt represented by the MMEs and the crust-derived felsic melt represented by the granitoid host (e.g., Chen et al. 2009a). Chappell (1996) and co-workers advocated a restitic origin for MMEs in granitoids from southeastern Australia (White and Chappell 1977; Chen et al. 1989; Chappell 1996), meaning that MMEs represented residues of partial melting. Nevertheless, the origin of MMEs remains a subject of debate (Dahlquist 2002;

Barbarin 2005; Niu et al. 2013).

The North Qilian orogenic belt (NQOB) at the northern margin of the Tibetan Plateau is a type suture zone of seafloor subduction and continental collision (Song et al. 2013). A general feature of the syncollisional granitoids in the NQOB is the presence of abundant MMEs of varying size dispersed randomly or in certain patterns (e.g., Niu et al. 2013), which offers an exceptional opportunity to study the petrogenesis of syncollisional granitoids and MMEs in orogenic belt. In this paper, we present a detailed case study of MMEs and the host Baojishan granodiorite in the eastern section of the NQOB. We critically evaluate the existing hypotheses by integrating petrology, zircon U-Pb geochronology, whole-rock major- and trace-element analysis, and Sr-Nd-Hf isotopic geochemistry. We conclude that the MMEs in this granodiorite do not provide evidence for magma mixing nor restite unmixing. Instead, we propose, on the basis of physical and chemical evidence, that the MMEs represent disturbed pieces of basal cumulate pile in response to the dynamics of newly replenished magmas as hypothesized by Niu et al. (2013).

Geological setting and petrography

The NQOB lies between the Alashan Block to the northeast and the Qilian Block to the southwest, and is offset to the northwest by the Altyn-Tagh Fault (Fig. 1a; e.g., Song et al. 2006, 2013). The NQOB is an Early Paleozoic suture zone, containing varying petrotectonic units formed at ridges, trenches, volcanic arcs and back arc systems (Xia et al. 2003). It comprises three subunits, (1) the southern ophiolite belt, (2) the middle arc magmatic belt and (3) the northern back-arc basin ophiolite-volcanic belt (Fig. 1a; Xia et al. 2003, 2012; Xia and Song 2010; Wu et al. 2011; Song et al. 2013; Chen et al. 2014). The well-preserved southern ophiolite subbelt extends from Aoyougou in the northwest, via Yushigou, Dongcaohe, to Yongdeng in the southeast, indicating seafloor spreading of the Qilian Ocean during ~ 560-500 Ma (Xiao et al. 1978; Shi et al. 2004; Tseng

et al. 2007; Song et al. 2009, 2013; Chen et al. 2014).

The Baojishan (BJS) granodiorite pluton is about 50km^2 in size and located in the eastern segment of the NQOB and the northern part of the magmatic arc belt (Fig. 1a). It makes up a ~180km NW-SE trending granitoid belt including Qumushan granodiorite (QG), Machangshan quartz diorite (MQD) and Laohushan quartz diorite (LQD) (Fig.1a) (Wang et al. 2006, 2008). It lies approximately 12 km to the southwest of Baoji town (Fig. 1a, b). The Baojishan (BJS) pluton intrudes the Ordovician sedimentary and metamorphic rocks of the Yingou Group (Fig. 1b) with a remarkably baked contact. It contains abundant MMEs. Our study focuses on the petrogenesis and implications of the MMEs by comparing them with their immediate host rocks.

The BJS pluton contains abundant MMEs of varying size (a few to 10s of centimeters) and shape in sharp contact with the granitoid host. The MMEs are dioritic and have the same mineralogy as the host granodiorite except that they are more abundant in mafic phases (e.g., amphibole and biotite) and finer-grained (Fig. 2a and 2b). For example, the MMEs contain plagioclase (~ 35% - 40%), amphibole (~ 40% - 50%), biotite (~ 5% - 15%), quartz (~ 5% - 20%), minor K-feldspar and accessory minerals such as apatite, sphene, zircon and Fe-Ti oxides. In contrast, the host granitoids contain less mafic phases (~ 5% - 10% amphibole, ~ 3%~10% biotite) and more felsic minerals (e.g., ~ 40% - 50% plagioclase, ~ 35% - 45% quartz) with similar accessory minerals. The MMEs show no chilled margins and textures of crystal resorption and reactive overgrowth, but mainly exhibit porphyritic-like textures, in which the amphibole crystals vary from euhedral to subhedral, indicating that they may represent concentrations of dense, early-formed phases (see Reid and Hamilton 1987); some plagioclase crystals show clear zoning.

Analytical methods

Zircon U-Pb dating

Zircon separation was done in laboratory of the Langfang Institute of Regional Geological Survey using a combined method of heavy liquid, magnetic and manual separation under a binocular. The selected zircons were set in an epoxy mount before polished to expose zircons in half depth. Cathodoluminescence (CL) images were taken at China University of Geosciences in Wuhan (CUGW), to examine the internal structure of individual zircon grains. Zircon U-Pb dating was done using LA-ICP-MS at CUGW. Laser sampling was performed using a GeoLas 2005. An Agilent 7500a ICP-MS instrument was used to acquire ion-signal intensities. Helium was applied as a carrier gas. The laser spot size was 32 μm. Zircon 91500 was used as external standard for U-Pb dating (Wiedenbeck et al. 1995), and analyzed twice between every 5 unknown analyses. NIST610 glass was used as an external standard to normalize U, Th and Pb concentrations of unknowns. The detailed analytical procedure follows Liu et al. (2010). The ages were calculated by using an in-house software ICPMSDataCal (ver. 8.0) (Liu et al. 2008). Common Pb correction was applied using the method of Andersen (2002). Age calculations and concordia plots were made using Isoplot (Ludwig 2003).

Mineral compositions

Mineral chemistry was determined using a JXA-8100 microprobe at Chang'an University, China. The operating conditions were 15 kV accelerating potential, probe current of 10 nA and beam diameter of 1 μm. The analytical details are following the quantitative analysis of silicate minerals by electron probe microanalysis of State Standard of the People's Republic of China (GB/T 15617-2002).

Major and trace elements

The whole-rock major and trace elements were determined at China University of Geosciences in Beijing (CUGB). Whole-rock major element oxides were analyzed using a Leeman Prodigy inductively coupled plasma-optical emission spectrometer (ICP-OES). Whole-rock trace elements were analyzed using an Agilent-7500a ICP-MS. Sample powders were digested using HF + HNO_3 in a high-pressure jacket equipped Teflon beaker in an oven for 48 hours to ensure complete digestion/dissolution. Rock standards GSR-1, GSR-3 and AGV-2 (US Geological Survey), and GSR-1 and GSR-3 (National geological standard reference materials of China) were used to monitor the analytical accuracy and precision. The analytic details and precisions are given in Song et al. (2010).

Whole-rock Sr-Nd-Hf isotopes

Whole-rock Sr-Nd-Hf isotopic analyses were done in the Radiogenic Isotope Facility at the University of Queensland, Australia. The rock powders were dissolved in a mixture of double-distilled concentrate HNO_3 and HF, and dried on a hot plate at 80°C. After converting any fluoride to nitrate, the dried residue was dissolved with 3 ml 2 N HNO_3 and 1.5 ml was loaded onto a stack of Sr-spec, Thru-spec and LN-spec resin columns to separate Sr, Nd, and Hf from the matrix, using a streamlined procedure modified after Mikova and Denkova (2007) and Yang et al. (2010). All measured $^{87}Sr/^{86}Sr$, $^{143}Nd/^{144}Nd$ and $^{176}Hf/^{177}Hf$ ratios were normalized to $^{86}Sr/^{88}Sr = 0.1194$, $^{146}Nd/^{144}Nd = 0.7219$ and $^{179}Hf/^{177}Hf = 0.7325$, respectively. Total procedural blanks are ~ 65, 60, and 16 pg for Sr, Nd and Hf, respectively. Analyses of NBS987 standard run during the same period gave $^{87}Sr/^{86}Sr = 0.710249 \pm 17$ (n=18, 2σ). In the course of $^{143}Nd/^{144}Nd$ and $^{176}Hf/^{177}Hf$ analysis, the in-house Nd standard, Ames Nd Metal and 10 ppm Hf ICP solution from Choice Analytical were used as instrument drift monitors, respectively. This in-house Nd Metal and Hf standards were cross-calibrated against the

JNdi-1 Nd international standard and the JMC-475 Hf international standard, respectively. Analyses of in-house Nd standard gave $^{143}Nd/^{144}Nd$ = 0.511966± 12 (n=24, 2σ), corresponding to a mean value of 0.282160 ± 6 (n = 16, 2σ) for JNdi-1 standard. Analyses of in-house Hf standard yielded a mean $^{176}Hf/^{177}Hf$ of 0.282146 ± 12 (n = 31, 2σ). The values of USGS reference materials JG-3 and BHVO-2 run with our samples are given in Appendix 1, which are consistent with the reported reference values (GeoREM, http://georem.mpch-mainz.gwdg.de/). Analytical details for sample digestion and Sr, Nd and Hf elemental column separation procedures are given in Guo et al. (2014).

Results

Zircon U–Pb ages

Two samples (i.e., a host-MME pair) were dated using zircon LA-ICP-MS U-Pb methods and the results are given in Table 1. In CL images (Fig. 3a), zircons from the host granodiorite (BJS12-04host) are transparent and colorless, mostly euhedral elongated crystals of 100–200 μm in length with length/width ratios of ~ 1:1-2:1 and show clear oscillatory zoning. Zircons from the host granodiorite have moderate Th (36-112 ppm), U (95-203 ppm), and Th/U ratios (0.32-0.59), which is consistent with being of magmatic origin (Hoskin and Schaltegger 2003). After rejecting discordant ages, zircons from host granodiorite yield a $^{206}Pb/^{238}U$ mean age of 433.7±3.4 Ma (1σ, n=13, MSWD = 0.23, Fig. 4a), representing the crystallization age (~430 Ma) of the granitoid host.

Zircons from the MMEs are transparent and colorless, mostly euhedral elongated crystals of 150–200 μm in length with length/width ratios of about 1:1-2:1, also showing clear oscillatory zoning in CL images (Fig. 3b). The Th content in these zircons ranges from 73 to 228 ppm and U from 173 to 369 ppm with Th/U ratios of 0.32-0.7. After rejecting discordant ages, zircons from the MMEs yield a $^{206}Pb/^{238}U$ mean age of 431.6±2.8 Ma (1σ, n=13, MSWD = 0.37, Fig. 4b), which is identical to the age of the host within analytical error, indicating

that both the MMEs and the host formed at the same time and may have a genetic link.

Mineral compositions

Carefully selected plagioclase and amphibole crystals were analyzed for major element composition using electron microprobe, in which Fe^{2+} and Fe^{3+} values of amphibole were re-calculated after Lin and Peng (1994).

Plagioclase

Plagioclase from the MMEs and their host granodiorite exhibit similar compositions with a large range of anorthite content (Table 2), and display similar normal zoning (Fig. 5a, 5b, 5c). Resorption textures or reversed zoning in plagioclase are often taken as reflecting changes in plagioclase stability brought about by magma mixing (e.g., Hibbard 1981), particularly when a new, more calcic plagioclase grows over the resorption zones (e.g., Vernon 1983, 1991; Pietranik and Koepke 2009, 2014; Chen et al. 2009a, 2009b, 2013; Ma et al. 2013). For example, when studying MMEs from the Taihang Mesozoic orogen in north China craton, Chen et al. (2009a, 2009b) proposed a process of magma mixing for their origin based on the observation of euhedral overgrowths of high-Ca plagioclase over low-Ca plagioclase. However, the lack of reversed zoning in our study suggests that mixing of compositionally different magmas is insignificant (or unlikely) in the petrogenesis of the MMEs and their host granodiorite we study.

Amphibole

Following Leake et al. (1997), amphiboles from the MMEs and their host granodiorite are compositionally the same and can be classified as calcic magnesiohornblende with high $Mg^{\#}$ (0.58-0.67) [$Mg^{\#}$= $Mg/(Mg+Fe^{2+})$] (Table 3, Fig. 6). They have medium SiO_2 (44.3~47.1wt.%), and low TiO_2 (0.57-1.45 wt. %), Na_2O (1.16-1.92 wt.%) and K_2O (0.26-1.92 wt.%). All the amphibole crystals of the MMEs and their host granodiorite are

compositionally uniform without zoning.

Bulk-rock major and trace elements

Major and trace elements data of whole rocks are given in Table 4. On the total alkalis-silica (TAS) diagram (Fig. 7a), the host rock samples plot in the granodiorite field. The MMEs plot in the fields of diorite, gabbro and gabbroic diorite, but they are petrologically amphibole-rich mafic-diorite with no pyroxene present. The host granodiorite samples are calc-alkaline (Fig. 7b) and metaluminous rocks with A/CNK of 0.96 - 1.0 (Fig. 7c), whereas the MMEs are high-K calc-alkaline to calc-alkaline (Fig. 7b) and metaluminous with A/CNK of 0.67 - 0.8 (Fig. 7c). The host granodiorite samples have relatively high SiO_2 (62.5 - 66 wt.%), Na_2O (3.36 - 3.42 wt.%), Al_2O_3 (15.5 - 16.8 wt.%), Mg# (0.55 - 0.59; Mg#=Mg/[Mg+Fe^{2+}]), Na_2O/K_2O (1.7 - 2.4). The MMEs on the other hand have low SiO_2 (52.95 - 58.45 wt.%), high Fe_2O_3, MgO, CaO and similar Mg# (0.57-0.59). They both have high Na_2O/K_2O ratios (1.7 - 2.4 for the host and 1.7 - 2.2 for the MMEs), and both are grossly I-type granitoids (Fig. 7c). On SiO_2-variation diagrams (Fig. 8), the MMEs and their host granodiorite define inverse linear trends for most elements (e.g., TiO_2, $Fe_2O_3^T$, MnO, MgO, CaO, Eu and Y abundances).

Chondrite-normalized REE patterns of the host granodiorite are scoop-shaped (Fig. 9a), showing highly and regularly fractionated patterns from La to Dy ($[La/Dy]_N$ = 4.8 - 13.9) and little to slightly fractionated patterns from Dy to Lu ($[Dy/Yb]_N \approx$ 1 - 1.1) without a garnet signature (i.e., no HREE depletion). Chondrite-normalized REE patterns of the MMEs are similar to their host granodiorite, but differ significantly in having elevated HREE abundances (Fig. 9a, 9b) because of their greater proportions of mafic minerals (e.g., amphibole and biotite) in which HREEs are less incompatible. The host granodiorite samples show a varying Eu anomaly of Eu/Eu* = 0.86 - 1.15, whereas the MMEs all have a negative Eu anomaly of Eu/Eu*=0.67 - 0.79 because of the lower plagioclase modes.

In the primitive mantle-normalized spidergram (Fig. 10), both the host samples and the MMEs are enriched in large ion lithophile elements (LILEs; e.g., Rb, K, Pb) and relatively depleted in high field strength elements (HFSEs; e.g., Nb, Ta, Ti) and show a varying Sr anomaly (i.e., Sr/Sr* = 0.9 - 2.2) for the host and a negative Sr anomaly (i.e., Sr/Sr* = 0.4 - 0.6) for the MMEs. The Nb/Ta ratios are sub-chondritic (vs. chondritic value of 17.5; Sun and McDonough 1989) and are the same for both the granodiorite host (15.1 - 16.1) and the MMEs (15.2 - 16.4).

Whole-rock Sr-Nd-Hf isotopes

Whole-rock Sr-Nd-Hf isotopic compositions for the MMEs and their host granodiorite are listed in Table 5. The $^{87}Sr/^{86}Sr$ initial ratios, $\varepsilon_{Nd}(t)$ and $\varepsilon_{Hf}(t)$ have been calculated at 430 Ma corresponding to the crystallization age of the MME-host granitoids (see above). The Sr-Nd isotope compositions for both the MMEs ($^{87}Sr/^{86}Sr_{(i)}$ = 0.7069 - 0.7082; $\varepsilon_{Nd}(t)$ = -3.9 - -3.1) and their host granodiorite ($^{87}Sr/^{86}Sr_{(i)}$ = 0.7067 - 0.7072; $\varepsilon_{Nd}(t)$ = -3.8 to -3.2) are quite similar and show a narrow range of variation (Fig. 11). The Hf isotope compositions of the MMEs and their host granodiorite exhibit a relatively wider range: in one host-MME pair (BJS12-08host/BJS12-08MME), the MME ($\varepsilon_{Hf}(t)$=6.4) has identical $\varepsilon_{Hf}(t)$ to the host ($\varepsilon_{Hf}(t)$=6.7) within analytical error. In another pair (BJS12-06host /BJS12-06MME), the MME ($\varepsilon_{Hf}(t)$=14.7) has more positive $\varepsilon_{Hf}(t)$ than the host ($\varepsilon_{Hf}(t)$=5.9), resulting from the too low Lu/Hf ratio (0.0196). The extremely high $\varepsilon_{Hf}(t)$ results from the calculation due to nugget effect of zircons (Van Dongen et al. 2010) because of the unexpectedly high Hf (3.53 ppm) and too high Zr (128 ppm); this cannot be readily discerned petrographically because of the accessory nature of zircons. A third pair (BJS12-10host/BJS12-10MME), the MME ($\varepsilon_{Hf}(t)$=1) has less positive $\varepsilon_{Hf}(t)$ than the host ($\varepsilon_{Hf}(t)$=5.8). Despite of a wide range of variation actually caused by the large variation of Lu/Hf ratios, the Hf isotope compositions for the MMEs and their host granodiorite are actually similar as the

Sr-Nd isotopes, because of the significant correlated variations of $^{87}Rb/^{86}Sr$ vs. $^{87}Sr/^{86}Sr$, $^{147}Sm/^{144}Nd$ vs. $^{143}Nd/^{144}Nd$, and $^{176}Lu/^{177}Hf$ vs. $^{176}Hf/^{177}Hf$ (Fig. 12). Contributions from mature continental crust are apparent as shown by the radiogenic Sr and unradiogenic Nd ($\varepsilon_{Nd}(t) < 0$), but the variably radiogenic Hf ($\varepsilon_{Hf}(t) > 0$) for both the MMEs and their host granodiorite also point to a significant mantle input. Theoretically, the present-day Nd and Hf isotopes of most crustal and mantle-derived rocks correlate and form the "Terrestrial Array" or Nd-Hf isotopic coupling (Vervoort et al. 1999, 2011) because of the similar behavior of radioactive parents (*P*: Sm and Lu) relative to radiogenic daughters (*D*: Nd and Hf), i.e., ($Kd_{[P/D]} > 1$: $Kd_{[Sm/Nd]} > 1$ and $Kd_{[Lu/Hf]} > 1$) during magmatism. However, the Nd-Hf isotopic decoupling is common and anticipated in granitoids (see Huang et al. 2014), especially if the source rock histories involve sedimentary and metamorphic processes because of (1) different half-life of the radioactive parents: $T_{1/2}(^{176}Lu) << T_{1/2}(^{147}Sm)$; (2) different behavior of Lu over Hf (vs. Sm over Nd); and the (3) "zircon effect" inherited from the source/protoliths histories (Patchett et al. 1984). Thus, Nd-Hf isotopes can exhibit decoupling in magmatic (granitoid) rocks inherited from sources involving non-magmatic processes (e.g., Huang et al. 2014). Although the exact controls on the observed Nd-Hf isotopic decoupling is significant and needs further exploration (see below), the most straightforward observation is that Sr-Nd-Hf isotopes between the MMEs and their host granodiorite are overlapping and indistinguishable, and show no correlated variations with SiO_2 and MgO (Fig. 13).

Discussion

Petrogenesis of the mafic magmatic enclaves

The MMEs have igneous mineralogy and textures, and have an identical age to their host granodiorite, indicating an igneous origin for the MMEs. This rules out the restite origin representing refractory residues of source-rock anatexis (e.g. White and Chappell 1977; Chen et al. 1989; Chappell 1996) at least for the BJS

MMEs which we study here as well as for those in many syncollisional granitoids which we are investigating at present (see Niu et al. 2013).

It is worth to note that the same or very similar observations mentioned above have been commonly used as evidence for magma mixing for MME-bearing granitoids (e.g. Vernon 1983; Didier 1987; Dorais et al. 1990; Castro et al. 1990; Barbarin and Didier 1991; Chen et al. 2009). However, in the case of BJS granitoids pluton, the magma mixing model has more difficulties than certainties. The correlated variations of TiO_2, $Fe_2O_3^T$, MnO, MgO, CaO with SiO_2 (Fig. 8) could be interpreted as reflecting magma mixing, but magma mixing is often considered a complex, multi-stage process (e.g., Clemens 1989; Bateman 1995) in which linear trends can be disturbed (Donaire et al. 2005). Furthermore, if the MMEs in the BJS pluton represent the basaltic melt for the magma mixing, the hypothetical magma parental to MMEs would be SiO_2-poor (<48wt.%), CaO-rich (>8.7wt.%) and MgO-rich (>8wt.%), but this is not the case and no such basaltic melt has been found in the study area. Importantly, the MMEs comprise dominantly amphibole and plagioclase, which are common cumulate minerals in andesitic melts. If the parental melts were basaltic, the typical cumulate from such evolved basaltic melt would be gabbro dominated by clinopyroxene and plagioclase. This is an important petrological concept. Because of the modal variability (amphibole vs. plagioclase; and MMEs vs. the host), these linear trends are consistent with mineral-mode-controlled mixing (Fig. 8) but it also consistent to first-order fractional crystallization (see below).

In this case, isotopes offer a robust tool for distinguishing mantle derived magmas (if the MMEs do represent such a magma with a mantle isotopic signature) from crustal melts (if the granitoid host does represent such a melt with a crustal isotopic signature) (Huang et al. 2014). For example, MMEs from Criffell and Strontian plutons in Great Britain (Holden et al. 1987) and felsic plutons in Taihang orogen (Chen et al. 2009b) have higher $\varepsilon_{Nd}(t)$ than the hosts, which may indeed have resulted from magma mixing. However, in the

case of our study, Sr-Nd-Hf isotopes between the MMEs and their host granodiorites are overlapping and indistinguishable, which is inconsistent with the origin of magma mixing between the alleged two different melts of mantle origin (represented by the MMEs) and crustal origin (represented by the granodiorite host), respectively. In spite of this, many authors still follow the popular view that thermal and chemical equilibration between coeval, compositionally contrasted magmas (Dorais et al. 1990; Eberz and Nicholls 1990; Allen 1991; Chen et al. 2009) can account for the similar isotopes between the two lithologies. We emphasize that it is physically unlikely that isotopes become homogenized whereas major and trace elements are not (Niu et al. 2013). This is simply because isotopes are "carried" by the relevant chemical elements and isotopic diffusion cannot take place without the diffusion of the "carrying" elements. Yet, some authors still argue that isotopic equilibration is generally more easily achieved than chemical equilibration (e.g., Barbarin, 2005) on the basis of some experimental interpretations (Lesher 1990). In the case of our study, there are two compelling arguments against thermal and chemical equilibration: (1) the MMEs are in sharp contact with their host granodiorite, and lack compositional or textural zoning related to their contacts; (2) plagioclase in the MMEs and their host granodiorite show no compositional and textural disequilibrium.

The foregoing analysis shows that MMEs in the BJS pluton formed from coeval and cognate magmas with their host granodiorite, rather than representing mantle derived magmas for magma mixing. Indeed, the cumulate origin for MMEs can overcome the difficulties of magma mixing and account for all of the observations: (1) the MMEs are mineralogically the same as their host granodiorite but have higher modes of mafic minerals (Amp and Bt) (Fig. 2), as they are products of early crystallization. This is actually consistent with experimental evidence that mafic minerals are the earliest liquidus phases crystalling prior to feldspars and quartz during granodioritic melt evolution (Naney and Swanson 1980); (2) the MMEs have higher abundances of HREEs than their host granodiorite (Fig. 9a, 9b) as they are enriched in mafic minerals; (3) the MMEs have

overlapping and indistinguishable Sr-Nd-Hf isotope composition with their host granodiorite as they both formed from the same magmas; (4) the coherent compositional trend on the SiO_2-variation diagrams is consistent with the liquid lines of descent (Fig. 8) and is directly controlled by the varying mineral modes.

However, the cumulate origin interpretation has been questioned since it was firstly proposed by Daly (1933), because it would not be consistent with the small grain size of MMEs (Barbarin and Didier 1991). To address this issue, Donaire et al. (2005) suggested that the MMEs forming processes would have been in zones of rapid cooling, e.g., at the walls of the magma conduits. The small grain size of MMEs is important and should be taken serious. However, it should not be regarded as independent evidence for magma mixing and against cumulate origin.

It is straightforward to perceive that emplacement of a body of primitive magma into a "cold" environment (e.g., developing a magma chamber), magma quench is inevitable when the wall-rock temperature is below the liquidus of the magma. For an andesitic primitive magma parental to the syncollisional granitoids (Niu et al. 2013), the first major liquidus phases would be amphibole (±biotite±plagioclase) and rapid quench will facilitate abundant nucleation without between-nuclei space for growth, thus forming fine-grained MME cumulate. This early fine-grained more mafic cumulate piles (largely plastic before complete solidification) can be disturbed by subsequently replenished granitoid (granodiorite and diorite) magmas with pieces of the cumulate included as MMEs in the granitoid host.

Constraints on the source

Implication from MMEs

It is likely that magma mixing is a common process in generating intermediate to felsic magmas worldwide. In the case of BJS pluton, however, we emphasize that contrary to the popular view, MMEs are not evidence for

magma mixing, but rather they are of cumulate origin (Niu et al. 2013). The argument for the origin of MMEs as magma mixing emphasized the role of mantle derived basaltic melt represented by the MMEs. However, the chemical characteristics and the petrology of the MMEs (e.g., lack of pyroxene and low An plagioclase) are consistent with the magmas parental to the MMEs and their host granodiorite being mafic andesite (Niu et al. 2013). In fact, our ongoing studies about the ~180 km long granitoid belt in the eastern segment of the NQOB (Fig. 1a) concur with the observations of the MMEs in BJS. This requires a volumetrically significant basaltic rock source to melt for the BJB MME-bearing granitoids.

Geochronological constraints

Recent studies suggested the Qilian ocean was closed at the end of the Ordovician (~445 Ma) followed by continental collision as recorded in subduction-zone metamorphic rocks on the northern edge of the Qilian–Qaidam block at ~ 435-420 Ma (see Song et al. 2013). The coeval (~430Ma) MMEs and their host granodiorite of BJS pluton are best interpreted as a magmatic response to the collision between the Qilian-Qaidam block and Alashan block. This analysis points to a genetic link between the magmatism and continental collision (Mo et al. 2008) for juvenile continental crust accretion and rules out the significance of intra-oceanic island arc or continental arc magmatism in space and time in continental crust accretion in the standard model.

Geochemical constraints

Following the foregoing data and discussion we tend to draw the conclusion that the primitive magmas parental to the BJS MME-bearing granodiorite are mafic andesitic magmas derived from a basaltic source during continental collision. In the broad context of the continental collision, possible basaltic source candidates in abundance are (1) recently accreted island arc complex (e.g. Kay and Kay 1993), (2) thickened lower crust (e.g. Xu et al. 2002; Chung et al. 2003; Wang et al. 2004, 2005a; Seghedi et al. 2007), and (3) the remaining part of

the oceanic crust (e.g. Niu 2005; Mo et al. 2008; Niu and O'Hara 2009).

It is noteworthy that the well preserved island-arc complex extends as a continuous belt between the two ophiolite belts along the major tectonic line of the NQOB (Zhang et al. 1998; Wang et al. 2005b; Xia et al. 2012; Song et al. 2013), apparently indicating the presence of an island-arc system in the North Qilian ocean before the continental collision. These well preserved island-arc complex seems to provide a probable basaltic source, however, it is not, because (1) island arcs with a positive topography are too shallow and too cold to melt (Niu et al. 2003); (2) melting of mafic/ultramafic deep arc crust cumulate, if there were any, could produce andesitic melt, but such melt would be too depleted (Mo et al. 2008; Tamura et al. 2009), in terms of the observed geochemistry of the BJS granodiorite (and the MMEs). Therefore, the recently accreted island arc complex cannot be the source for the BJS MME-bearing granodiorite.

Recently, many adakitic rocks derived from the lower crust in mainland China and on the Tibetan Plateau have been reported. The geochemistry (e.g., high Sr/Y, La/Yb ratios and depleted HREE) of these adakitic intrusive rocks suggests that garnet must have been stable as a residual phase during partial melting (e.g., Xu et al. 2002; Wang et al. 2004, 2006; Chung et al. 2003). However, the scoop-shaped chondrite normalized REE patterns (Fig. 9a) and the constant $(Dy/Yb)_N$ with increasing $(La/Sm)_N$ (Fig. 14) of the BJS pluton, indicate that garnet was not present, which contradicts with the geochemical signatures formed by partial melting of lower crustal garnet amphibolite or eclogite. Moreover, the positive $\varepsilon_{Hf}(t)$ values require significant mantle input, which is distinct from reported adakitic rocks derived from the lower crust (see Castillo 2012 for review). Thus, the origin by partial melting of the pre-existing lower crust is implausible.

In this case, the remaining part of the North Qilian oceanic crust seems to be the most likely source for generating andesitic magmas parental to the BJS pluton, because it can inherit the mantle isotopic signatures from its source (asthenospheric mantle). In spite of this, melting of the remaining part of North Qilian oceanic

crust, if it can account for the origin of QMS pluton successfully, must be able to explain two basic issues.

First, what mechanism and condition may have caused melting of the remaining part of the North Qilian oceanic crust? A reasonable mechanism in a syn-collisional setting has been proposed by Mo et al. (2008) and can be addressed through physical, petrological and geochemical studies (Mo et al. 2008; Niu and O'Hara 2009; Niu et al. 2013). In their model, during collision, the underthrusting oceanic crust would subduct/underthrust slowly, tend to attain thermal equilibrium with the superjacent warm active continental margin, and evolve along a high T/P path in P-T space. The warm hydrated oceanic crust and sediments would melt when reaching the hydrous basaltic solidus under the amphibolite facies conditions. Indeed, there are many geochemical similarities between the magmas parental to the BJS MME-bearing granodiorite and the melts produced from such a mechanism, including (1) andesitic composition; (2) mantle (vs. crustal) dominated isotopic signatures inherited from the oceanic crust (actually ~95% mantle contribution, Fig. 11); (3) no garnet signature, e.g., non-to slightly fractionated REE from Ho to Lu ($[Dy/Yb]_N$ =1~1.1), which are most likely an amphibole signature (as residual phase or fractional crystallization) rather than garnet (Fig. 14). This is identical with oceanic crust melted under amphibolite (vs. eclogite) phase conditions without garnet presence; (4) having an "arc-like signature", i.e., relative depletion in Nb, Ta and Ti (Fig. 10), because these HFSEs are compatible in ilmenite (or pseudobrookite), which is a common phase in amphibolite (Niu and Lesher 1991) and its refractory property make it a residual phase holding these elements (Mo et al. 2008); (5) sub-chondritic Nb/Ta ratio (15.1 - 16.1) because of amphibole controlled fractionation ($Kd^{Nb/Ta}_{amphibole}$ =1.40) (Foley et al. 2002).

Second, what processes slightly enriched the depleted andesitic melts in $^{87}Sr/^{86}Sr(i)$ and εNd(t) while $\varepsilon_{Hf}(t)$ values maintained its inherited depleted signature? Briefly, what kind of processes decoupled the Nd-Hf isotope systems during generation or evolution of the andesitic melts? Obviously, contribution from continental crust is required, while it may occur in the melting region or an evolving magma chamber rather than simple crustal

level assimilation, as the Sr-Nd-Hf isotopes for the MMEs and their host granodiorites are closely similar and show a respectively narrow range of variation, and they do not show correlated variations with SiO_2 and MgO (Fig. 13). Melting of recycled terrigenous sediments of upper continental crust and remaining part of the North Qilian oceanic crust in the melting region is more likely (Mo et al. 2008; Niu and O'Hara 2009; Huang et al. 2014). Note that this assumption is consistent with simple binary isotope mixing calculations. In Fig. 11, the MMEs and their granodiorite isotopic data plot along a two-component "mixing" trend between the North Qilian oceanic crust and terrigenous sediments. In the calculation, the North Qilian oceanic crust is represented by the ophiolitic MORB in Yushigou, Jiugequan, Dachadaban and Laohushan, NQOB (Hou et al. 2006a, 2006b), and terrigenous sediment is represented by the Mohe gneiss (Chen et al. 2007; Li et al. 2007). The isotopic compositions of the two end-members are given in Table 6. The apparent decoupling between Nd and Hf isotopes was caused by the large difference in Nd/Hf ratios between the sediment and the oceanic crust which makes the mixing line highly curved and shift away from the terrestrial array (Fig. 11) (e.g., Huang et al. 2014). Taking consideration of mass balance, the contribution of mantle (i.e., the North Qilian MORB) is ~95%, and the contribution of terrigenous sediments (i.e., the Mohe gneiss) is ~5%.

Hence, partial melting of recycled terrigenous sediments and the remaining part of North Qilian oceanic crust during the collision under the amphibolite facies conditions can readily explain the source of the BJS MME-bearing granodiorite.

Conclusions

1. Zircon U-Pb ages of the host granodiorite (433.7±3.4 Ma) and their contained MMEs (431.6±2.8 Ma) coincide with the closure of the Qilian ocean and continental collision at ~440-420Ma. This indicates that the granitoids must be a magmatic response to the collision between the Qilian-Qaidam block and Alashan block.

2. The MMEs have the same crystallization age, very similar isotopic composition and the same mineralogy with their host granodiorite i.e. they are co-genetic. We conclude that the MMEs are cumulate rocks formed at earlier stages of the same magmatic systems rather than representing mantle melt required by the popular and the alleged magma mixing model.

3. The radiogenic Sr and unradiogenic Nd ($\varepsilon_{Nd}(t) < 0$) indicate the contribution of mature continental crust, while variably radiogenic Hf ($\varepsilon_{Hf}(t) > 0$) for both the MMEs and their host granodiorite also point to a significant mantle input. The apparent decoupling between Nd and Hf isotopes was caused by partial melting of recycled terrigenous sediments and the remaining part of North Qilian oceanic crust during collision.

Acknowledgements

This work was supported by the National Natural Science Foundation of China (NSFC: 91014003, 41130314) and two geological survey projects of China Geological Survey Departments and Offices (1212011121092, 1212011220928). We thank Yongsheng Liu and Zhaochu Hu for assistance with zircon analysis, Li Su with whole rock major and trace elements analysis, Minwu Liu with electron microprobe analysis, and Jianxin Zhao and Yuexing Feng with hole-rock Sr-Nd-Hf isotope analysis.

References

Allen CM (1991) Local equilibrium of mafic enclaves and granitoids of the Turtle Pluton, Southeast California: mineral, chemical, and isotopic evidence. Am Mineral 76: 574-588

Andersen T (2002) Correction of common lead in U–Pb analyses that do not report ^{204}Pb. Chem Geol 192: 59–79

Bateman R (1995) The interplay between crystallization, replenishment and hybridization in large felsic magma

chambers. Earth-Sci REV 39: 91-106

Barbarin B, Didier J (1991) Enclaves of the Mesozoic calc-alkaline granitoids of the Sierra Nevada batholith, California-. In: Didier J, Barbarin B. (Ed) Enclaves and Granite Petrology, Elsevier, Amsterdam, pp 135–153.

Barbarin B (2005) Mafic magmatic enclaves and mafic rocks associated with some granitoids of the central Sierra Nevada batholith, California: nature, origin, and relations with the hosts. Lithos 80: 155-177

Brenan JM, Shaw HF, Ryerson FJ, Phinney DL (1995) Experimental determination of trace-element partitioning between pargasite and a synthetic hydrous andesitic melt. Earth Planet Sci Lett 135: 1-11

Castro A, Morenoventas I, Delarosa JD (1990) Microgranular enclaves as indicators of hybridization processes in granitoid rocks, Hercynian Belt, Spain. Geol J 25: 391-404

Chappell BW, White AJR, Wyborn D (1987) The importance of residual source material (restite) in granite petrogenesis. J Petrol 28: 1111-1138

Castillo P R (2012) Adakite petrogenesis. Lithos 134: 304-316.

Chappell BW (1996) Magma mixing and the production of compositional variation within granite suites: evidence from the granites of southeastern Australia. J Petrol 37: 449-470

Chauvel C, Lewin E, Carpentier M, Arndt NT, Marini JC (2007) Role of recycled oceanic basalt and sediment in generating the Hf–Nd mantle array. Nature Geosci 1: 64-67

Chen B, Chen ZC, Jahn BM (2009a) Origin of mafic enclaves from the Taihang Mesozoic orogen, north China craton. Lithos 110: 343-358

Chen B, He J, Ma X (2009b) Petrogenesis of mafic enclaves from the north Taihang Yanshanian intermediate to felsic plutons: Evidence from petrological, geochemical, and zircon Hf-O isotopic data. Sci China Earth Sci 52: 1331-1344

Chen B, Jahn BM, Suzuki K (2013) Petrological and Nd-Sr-Os isotopic constraints on the origin of high-Mg adakitic rocks from the North China Craton: Tectonic implications. Geology 41: 91-94

Chen YD, Price RC, White AJR (1989) Inclusions in three S-type granites from southeastern Australia. J Petrol 30: 1181-1218

Chen YX, Song SG, Niu YL, Wei CJ (2014) Melting of continental crust during subduction initiation: A case study from the Chaidanuo peraluminous granite in the North Qilian suture zone. Geochim Cosmochim Acta 132: 311-336

Chung SL, Liu D, Ji J, Chu MF, Lee HY, Wen DJ, Zhang Q (2003) Adakites from continental collision zones:

melting of thickened lower crust beneath southern Tibet. Geology 31: 1021-1024

Clemens JD, Wall VJ (1988) Controls on the mineralogy of S-type volcanic and plutonic rocks. Lithos 21: 53-66

Dahlquis, JA (2002) Mafic microgranular enclaves: early segregation from metaluminous magma (Sierra de Chepes), Pampean Ranges, NW Argentina. Journal of South American Earth Sciences 15: 643-655

Daly RA (1933) Igneous rocks and the depth of the earth McGraw-Hill, New York, p 598

Defant MJ, Drummond MS, 1990 Derivation of some modern arc magmas by melting of young subducted lithosphere. Nature 347: 662-665

Didier J (1973) Granites and their enclaves: the bearing of enclaves on the origin of granites ~~(p 393) Amsterdam: Elsevier~~

Didier J (1987) Contribution of enclave studies to the understanding of origin and evolution of granitic magmas. Geologische Rundschau 76: 41-50

Dodge FCW, Kistler RW (1990) Some additional observations on inclusions in the granitic rocks of the Sierra Nevada. J Geophys Res 95: 17841-17848

Dorais MJ, Whitney JA, Roden Mf (1990) Origin of mafic enclaves in the Dinkey Creek pluton, central Sierra Nevada batholith, California. J Petrol 31: 853-881

Donaire T, Pascual E, Pin C, Duthou JL (2005) Microgranular enclaves as evidence of rapid cooling in granitoid rocks: the case of the Los Pedroches granodiorite, Iberian Massif, Spain. Contrib Mineral Petrol 149: 247-265

Dreher ST, Macpherson CG, Pearson DG, Davidson JP (2005) Re-Os isotope studies of Mindanao adakites: Implications for sources of metals and melts. Geology 33: 957-960

Eberz GW, Nicholls IA (1990) Chemical modification of enclave magma by post-emplacement crystal fractionation, diffusion and metasomatism. Contrib Mineral Petrol 104: 47-55

Faure G (1977) Principles of isotope geology. John Wiley & Sons, USA.

Fourcade S, Allegre CJ (1981) Trace elements behavior in granite genesis: A case study. The calc-alkaline plutonic association from the Querigut complex (Pyrénées, France). Contrib Mineral Petrol 76: 177-195

Foley S, Tiepolo M, Vannucci R (2002) Growth of early continental crust controlled by melting of amphibolite in subduction zones. Nature 417: 837-840

Guo PY, Niu YL, Ye L, Liu JJ, Sun P, Cui HX, Zhang Y, Gao JP, Su L, Zhao JX, Feng YX (2014) Lithosphere

thinning beneath west North China Craton: Evidence from geochemical and Sr-Nd-Hf isotope compositionsof Jining basalts. Lithos 202/203: 37-54

Hibbard MJ (1981) The magma mixing origin of mantled feldspar. Contrib Mineral Petrol 76:158–170

Hoskin PW, Schaltegger U (2003) The composition of zircon and igneous and metamorphic petrogenesis. Rev Mineral Geochem 5: 27-62

Hou QY, Zhao ZD, Zhang HF, Zhang BR, Chen YL (2006a) Indian Ocean-MORB-type isotopic signature of Yushigou Ophiolite in north Qilian Mountains and its implications. Sci China Earth Sci 49: 561–572

Hou QY, Zhao ZD, Zhang BR (2006b) On the boundary of Tethyan tectonic domain at the northeastern margin of the Tibetan Plateau. Geochim Cosmochim Acta 22: 567-577

Holden P, Halliday AN, Stephens WE (1987) Neodymium and strontium isotope content of microdiorite enclaves points to mantle input to granitoid production. Nature 330: 53-55

Huang H, Niu YL, Nowell G, Zhao ZD, Yu XH, Zhu DC, Mo XX, Ding S (2014) Geochemical constraints on the petrogenesis of granitoids in the East Kunlun Orogenic belt, northern Tibetan Plateau: Implications for continental crust growth through syn-collisional felsic magmatism. Chem Geol 370: 1-18

Kay RW, Kay SM (1993) Delamination and delamination magmatism. Tectonophysics 219: 177-189

Klein M, Stosch HG, Seck HA (1997) Partitioning of high field-strength and rare-earth elements between amphibole and quartz-dioritic to tonalitic melts: an experimental study. Chem Geol 138: 257-271

Leake BE, Wooley AR, Arps CES, Birch WD, Gilbert MC, Grice JD, Hawthorne, FC, Kato A, et al. (1997) Nomenclature of amphiboles: report of the Subcommittee on Amphiboles of the International Mineralogical Association, commission on new minerals and mineral names. Can Mineral 35: 219–246

Le Maitre RW, Streckeisen A, Zanettin B, Le Bas MJ, Bonin B, Bateman P (2005) Igneous Rocks: a classification and glossary of terms. Cambridge University Press, Cambridge, UK

Lesher CE (1990) Decoupling of chemical and isotopic exchange during magma mixing. Nature 344: 235-237

Li XY, Chen NS, Xia XP, Sun M, Xu P, Wang QY, Wang XY (2007) Constaints on timing of the early-Paleoproterozoic magmatism and crustal evolution of the Oulongbuluke micricontinent: U-Pb and Lu-Hf isotope systematics of zircons from Mohe granitic pluton. Acta Petrol Sinica 23: 513-522 (In Chinese with English abstract)

Lin WW, Peng LJ (1994) The estimation of Fe^{3+} and Fe^{2+} contents in amphibole and biotite from EMPA data. Journal of Changchun University Earth Sciences 24: 155–162 (in Chinese with English abstract)

Liu YS, Zong KQ, Kelemen PB, Gao S (2008) Geochemistry and magmatic history of eclogites and ultramafic rocks from the Chinese continental scientific drill hole: Subduction and ultrahigh-pressure metamorphism of lower crustal cumulates. Chem Geol 247: 133-153

Liu YS, Gao S, Hu ZC, Gao CG, Zong KQ, Wang DB (2010) Continental and oceanic crust recycling-induced melt peridotite interactions in the trans-North China Orogen: U–Pb dating, Hf isotopes and trace elements in zircons from mantle xenoliths. J Petrol 51: 537–571

Ludwig KR (2003) Isoplot/Ex Version 3.00: a Geochronological Toolkit for Microsoft Excel. Berkeley Geochronology Center, Berkeley, CA, USA

Ma X, Chen B, Chen JF, Niu XL (2013) Zircon SHRIMP U-Pb age, geochemical, Sr-Nd isotopic, and in-situ Hf isotopic data of the Late Carboniferous-Early Permian plutons in the northern margin of the North China Craton. Sci China Earth Sci 56: 126-144

Mikova J, Denkova P (2007) Modified chromatographic separation scheme for Sr and Nd isotope analysis in geological silicate samples. J Geosci 52: 221–226

Mo XX, Niu YL, Dong GC, Zhao ZD, Hou ZQ, Zho, S, Ke S (2008) Contribution of syncollisional felsic magmatism to continental crust growth: a case study of the Paleogene Linzizong volcanic succession in southern Tibet. Chem Geol 250: 49-67

Naney MT, Swanson SE (1980) The effect of Fe and Mg on crystallization in granitic systems. Am Mineral 65: 639-653

Niu YL (2005) Generation and evolution of basaltic magmas: some basic concepts and a new view on the origin of Mesozoic–Cenozoic basaltic volcanism in eastern China. J China Univ 11: 9-46

Niu YL, Lesher CM (1991) Hydrothermal alteration of mafic metavolcanic rocks and genesis of Fe-Zn-Cu sulfide deposits, Stone Hill district, Alabama. Econ Geol 86: 983-1001

Niu YL, O'Hara MJ (2003) Origin of ocean island basalts: A new perspective from petrology, geochemistry, and mineral physics considerations. J Geophys Res 108: 1-19

Niu YL, O'Hara MJ, Pearce JA (2003) Initiation of subduction zones as a consequence of lateral compositional buoyancy contrast within the lithosphere: a petrologic perspective. J Petrol 44: 851-866

Niu, YL, O'Hara MJ (2009) MORB mantle hosts the missing Eu (Sr, Nb, Ta and Ti) in the continental crust: new perspectives on crustal growth, crust–mantle differentiation and chemical structure of oceanic upper mantle. Lithos 112: 1-17

Niu YL, Zhao ZD, Zhu DC, Mo XX (2013) Continental collision zones are primary sites for net continental

crust growth - A testable hypothesis. Earth Sci REV 127: 96-110

Pabst A (1928) Observations on inclusions in the granitic rocks of the Sierra Nevada. University of California Publications 17: 325– 386

Patchett PJ, White WM, Feldmann H, Kienlinczuk S, Hofmann AW (1984) Hafnium/rare earth element fractionation in the sedimentary system and crustal recycling into the Earth's mantle. Earth Planet Sci Lett 69: 365-378

Peccerillo A, Taylor SR (1976) Geochemistry of Eocene calc-alkaline volcanic rocks from the Kastamonu area, northern Turkey. Contrib Mineral Petrol 58: 63–81

Phillips JA (1880) On concretionary patches and fragments of other rocks contained in granites. Quarterly J Geol Soc 3: 1-22

Pietranik A, Koepke J (2009) Interactions between dioritic and granodioritic magmas in mingling zones: plagioclase record of mixing, mingling and subsolidus interactions in the Gęsiniec Intrusion, NE Bohemian Massif, SW Poland. Contrib Mineral Petrol 158: 17-36

Pietranik A, Koepke J (2014) Plagioclase transfer from a host granodiorite to mafic microgranular enclaves: diverse records of magma mixing. Miner Petrol 108: 681–694

Reid Jr, JB, Hamilton, MA (1987) Origin of Sierra Nevadan granite: evidence from small scale composite dikes. Contrib Mineral Petrol 96: 441-454

Rudnick RL, Gao S (2003) Composition of the continental crust. Treatise Geochem 3: 1-64

Ronov AB, Yaroshevsky AA (1976) A new model for the chemical structure of the Earth's crust. Geochem Int 13: 89-121.

Seghedi I, Bojar AV, Downes H, Roşu E, Tonarini S, Mason P (2007) Generation of normal and adakite-like calc-alkaline magmas in a non-subductional environment: An Sr-O-H isotopic study of the Apuseni Mountains Neogene magmatic province, Romania. Chem Geol 245: 70-88

Schmidt MW (1992) Amphibole composition in tonalite as a function of pressure: an experimental calibration of the Al-in-hornblende barometer. Contrib Mineral Petrol 110: 304-310

Sisson TW, Ratajeski K, Hankins WB, Glazner AF (2005) Voluminous granitic magmas from common basaltic sources. Contrib Mineral Petrol 148: 635-661

Shi RD, Yang JS, Wu CL (2004) First SHRIMP dating for the formation of the Late Sinian Yushigou Ophiolite North Qilian Mountains. Acta Geol Sinica, 78: 649-657 (in Chinese with English abstract)

Slaby E, Götze J (2004) Feldspar crystallization under magma-mixing conditions shown by

cathodoluminescence and geochemical modelling - a case study from the Karkonosze pluton (SW Poland). Mineral Mag 68: 561-577

Song SG, Zhang LF, Niu YL, Su L, Song B, Liu DY (2006) Evolution from oceanic subduction to continental collision: a case study from the Northern Tibetan Plateau based on geochemical and geochronological data. J Petrol 47: 435-455

Song SG, Su L, Niu YL, Lai Y, Zhang LF (2009) CH_4 inclusions in orogenic harzburgite: evidence for reduced slab fluids and implication for redox melting in mantle wedge. Geochim Cosmochim Acta 73: 1737-1754

Song SG, Su L, Li XH, Zhang GB, Niu YL, Zhang LF (2010) Tracing the 850-Ma continental flood basalts from a piece of subducted continental crust in the North Qaidam UHPM belt, NW China. Precamb Res 183: 805-816

Song SG, Niu YL, Su L, Xia XH (2013) Tectonics of the North Qilian orogen, NW China. Gondwana Res 23: 1378-1401

Sun SS, McDonough W (1989) Chemical and isotopic systematics of oceanic basalts: implications for mantle composition and processes. Geol Soc London Spec Publ 42: 313-345

Tamura Y, Gill JB, Tollstrup D, Kawabata H, Shukuno H, Chang Q, Kodaira S, Ishizuka O, Suzuki T, Kido Y, Fiske RS, Tatsumi Y (2009) Silicic magmas in the Izu–Bonin oceanic arc and implications for crustal evolution. J Petrol 50: 685-723

Tatsumi Y (2006) High-Mg andesites in the Setouchi volcanic belt, s*outh*western Japan: analogy to Archean magmatism and continental crust formation? Annu Rev Earth Planet Sci 34: 467-499

Tseng CY, Yang HJ, Yang HY, Liu D, Tsai CL, Wu H, Zuo G (2007) The Dongcaohe ophiolite from the North Qilian Mountains: a fossil oceanic crust of the Paleo-Qilian ocean. Chin Sci Bull 52: 2390-2401

Tseng CY, Yang HJ, Yang HY, Liu D, Wu C, Cheng CK, Chen CH, Ker CM (2009) Continuity of the North Qilian and North Qinling orogenic belts, Central Orogenic System of China: Evidence from newly discovered Paleozoic adakitic rocks. Gondwana Res 16: 285-293

Van Dongen M, Weinberg RF, Tomkins AG (2010) REE-Y, Ti, and P remobilization in magmatic rocks by hydrothermal alteration during Cu-Au deposit formation. Econ Geol, 105: 763-776.

Vernon RH (1983) Restite, xenoliths and microgranitoid enclaves in granites. Journal and Proceedings of the Royal Society of New South Wales 116: 77–103

Vernon RH (1991) Interpretation of microstructures of microgranitoid enclaves In: Didier J, Barbarin B (eds)

Enclaves and granite petrology. Elsevier, Amsterdam pp 277-291

Vervoort JD, Blichert-Toft, J (1999) Evolution of the depleted mantle: Hf isotope evidence from juvenile rocks through time. Geochim Cosmochim Acta 63: 533-556

Vervoort JD, Plank T, Prytulak J (2011) The Hf–Nd isotopic composition of marine sediments. Geochim Cosmochim Acta 75: 5903-5926

Wang Q, Xu JF, Zhao ZH, Bao ZW, Xu W, Xiong XL (2004) Cretaceous high-potassium intrusive rocks in the Yueshan-Hongzhen area of east China: Adakites in an extensional tectonic regime within a continent. Geochem J 38: 417-434

Wang Q, McDermott F, Xu JF, Bellon H, Zhu YT (2005a) Cenozoic K-rich adakitic volcanic rocks in the Hohxil area, northern Tibet: lower-crustal melting in an intracontinental setting. Geology 33: 465-468

Wang CY, Zhang Q, Qian Q, Zhou MF (2005b) Geochemistry of the Early Paleozoic Baiyin volcanic rocks (NW China): implications for the tectonic evolution of the North Qilian orogenic belt. J Geol 113: 83-94

Wang JR, Wu CJ, Cai ZH, Guo YS, Wu JC, Liu XH (2006) Early Paleozoic high-Mg adakite froin Yindongliang in the eastern section of the North Qilian: Implications for geodynamics and Cu-Au mineralization. Acta Petrol Sinica 22: 2655-2664 (in Chinese with English abstract)

Wang JR, Wu JC, Jia ZL (2008) Sujiashan high-Mg adakite in the eastern section of North Qilian Mountains: implications for geodynamics. J Lanzhou Univ 44: 16-23 (in Chinese with English abstract)

Watson EB, Wark DA, Thomas JB (2006) Crystallization thermometers for zircon and rutile. Contrib Mineral Petrol 151: 413-433

Wiedenbeck M, Alle P, Corfu F, Griffin WL, Meier M, Oberli F, Quadt A, Roddick JC, Spiegel W (1995) Three natural zircon standards for U−Th−Pb, Lu−Hf, trace element and REE analyses . Geostand Newslett 19: 1-23

Wu FY, Li XH, Zheng YF, Gao S (2007) Lu-Hf isotopic systematics and their applications in petrology. Acta Petrol Sinca 23: 185-220 (in Chinese with English abstract)

White AJ, Chappell BW (1977) Ultrametamorphism and granitoid genesis. Tectonophysics 43: 7-22

Wu C, Gao Y, Frost BR, Robinson PT, Wooden JL, Wu SP, Chen QL, Lei M (2011) An early Palaeozoic double-subduction model for the North Qilian oceanic plate: evidence from zircon SHRIMP dating of granites. Int Geol Rev 53: 157-181

Xia LQ, Xia ZC, Xu XY (2003) Magma genesis in the Ordovician backarc basins of the Northern Qilian

Mountains, China. Geol Soc Am Bull 115: 1510-1522

Xia XH, Song SG (2010) Forming age and tectono-petrogenesis of the Jiugequan ophiolite in the North QilianMountain, NW China. Chin Sci Bull 55: 1899-1907 (in Chinese with English abstract)

Xia XH, Song SG, Niu YL (2012) Tholeiite-boninite terrane in the North Qilian suture zone: implications for subduction initiation and back-arc basin development. Chem Geol 32: 259–277

Xiao XC, Chen GM, Zhu ZZ (1978) A preliminary study on the tectonics of ancient ophiolites in the Qilian Mountain, Northwest China. Acta Geol Sinica 52: 281-295 (in Chinese with English abstract)

Xu JF, Shinjo R, Defant MJ, Wang Q, Rapp RP (2002) Origin of Mesozoic adakitic intrusive rocks in the Ningzhen area of east China: partial melting of delaminated lower continental crust? Geology 30: 1111-1114

Xu ZQ, Xu HF, Zhang JX, Zhao JX, Li HB, Zhu ZZ, Qu JC, Chen DZ, Chen JL, Yang KC (1994) The Zhoulangnashan Caledonian subductive complex in the Northern Qilian Mountains and its dynamics. Acta Geol Sinica 68: 1-15 (in Chinese with English abstract)

Yang ZF, Luo ZH, Zhang HF, Zhang YM, Huang F, Sun CG, Dai JG (2009) Petrogenesis and geological implications of the Tianheyong Cenozoic basalts, Inner Mongolia, China. Earth Sci Front 16: 90–106

Zhang JJ，Wang GJ，Yang XY, Sun WD, Dai SQ (2012) The petrogenesis of the Jingde granodiorite and its MMEs: Constraints from geochemistry，zircon U-Pb dating and Hf isotopic compositions. Acta Petrol Sinica 28: 4047- 4063 (in Chinese with English abstract)

Zhang Q, Chen Y, Zhou D, Qian Q, Jia X, Han S (1998) Geochemical characteristics and genesis of Dachadaban ophiolite in North Qilian area. Sci China Earth Sci 41: 277-281

Zindler A, Hart S (1986) Chemical geodynamics. Ann Rev Earth Planet Sci 14: 493-571

Figure Captions

Fig. 1. (a) Simplified geological map of the North Qilian Orogen showing the main tectonic units (after Song et al. 2013), whose geographic location in continental China is shown in the inset. (b) Simplified map of the Baojishan (BJS) area in the eastern section of the North Qilian Orogen.

Fig. 2. Photographs showing the Baojishan granodiorite with mafic magmatic enclaves (MMEs). (a) and (b) showing the sharp contact of MMEs with their host granodiorite, and MMEs are finer-grained than the host; (b), (c) and (d) showing the same mineralogy between the host granodiorite (c) and their MMEs (d) except that the MMEs have greater mafic mineral modes.

Fig. 3. Representative CL images of zircon grains showing spots for zircon U-Pb dating using LA-ICP-MS and weighted mean ages in Ma for a granodiorite host (a, BJS12-04host) and its MME (b, BJS12-04MME).

.

Fig. 4. Concordia diagrams of U-Pb zircon age data for a granodiorite host (a; BJS12-04host) and its MME (b; BJS12-04MME).

Fig. 5. Plagioclase composition in terms of anorthite content (An) in granodiorite hosts (a, BJS12-08host; b, BJS12-04host) and the MME (c, BJS12-04MME). See Table 2 for compositional data.

Fig. 6. Chemical compositions of amphiboles from the host granodiorite and MMEs in the amphibole classification diagram (Leake et al. 1997).

Fig. 7. Comparison of Baojishan granodiorite and MME compositions in diagrams of (a) The total alkali vs. SiO_2 (TAS; Le Maitre et al. 2005), (b) K_2O *vs.* SiO_2 (Peccerillo and Taylor 1976), and (c) A/NK *vs.* A/CNK.

Fig. 8. Harker diagrams of major element oxides *vs.* SiO_2 for the Baojishan host granodiorites and the MMEs, showing compositional controls of modal mineralogy and varying extent of fractional crystallization (cumulate for MMEs and "residual" melt for the host; see text for details). Bulk continental crust (BCC) composition (Rudnick and Gao 2003) is plotted for comparison.

Fig. 9. (a) Chondrite normalized REE patterns for the Baojishan host granodiorites and the MMEs; (b) host rock-normalized REE diagrams of MMEs, each MME has been normalized with regard to its specific host. Chondrite REE values are from Sun and McDonough (1989).

Fig. 10. (a) Average ocean crust (OC; Niu and O'Hara, 2003) normalized incompatible element spidergram for the Baojishan host granodiorites and the MMEs.

Fig. 11. Plot of $\varepsilon_{Nd}(t)$ *vs.* $^{87}Sr/^{86}Sr_{(i)}$ (a) and $\varepsilon_{Nd}(t)$ *vs.* $\varepsilon_{Hf}(t)$ (b) for the Baojishan host granodiorites and the MMEs, showing that they all have indistinguishable isotopic compositions and plot along an apparent 'mixing' trend between North Qilian Ocean MORB and terrestrial sediments (the Mohe gneiss). The terrestrial array is from Chauvel et al. (2008). Isotopic compositions of the two geochemical end-members are given in Table 6. The isotopic mixing line calculated after Faure (1977) with 10% intervals shown.

Fig. 12. Present-day pseudochrons for samples from Baojishan granitoids. (a) Rb/Sr vs. $^{87}Sr/^{86}Sr$, yielding 648 Ma, (b) Sm/Nd vs. $^{143}Nd/^{144}Nd$, yielding 382 Ma, and (c) Lu/Hf vs. $^{176}Hf/^{177}Hf$, yielding 327 Ma. Note that Sm-Nd and Lu-Hf pseudo-chron ages are close to the zircon in situ dating age of ~430 Ma.

Fig. 13. Plot of Sr-Nd-Hf isotopes *vs.* MgO and SiO_2, showing overlapping isotopes between MMEs and their granodiorite hosts, and they show no correlated variations with SiO_2 or MgO.

Fig. 14. Plot of $(La/Sm)_N$ vs. $(Dy/Yb)_N$, showing Rayleigh fractional crystallization trends (10% melt increment) of garnet, amphibole, plagioclase, and 90% amphibole+10% garnet were calculated to show an amphibole signature rather than garnet. The parental magma is assumed to have La, Sm, Dy and Yb contents identical to BCC for convenience. The partition coefficients for amphibole and garnet are from Klein et al. (1997) and Ronov and Yaroshevskiy (1976), respectively. Data source of adakitic rocks are from Xu et al. (2002) and Wang et al. (2005a).

Table Captions

Table 1: LA-ICP-MS zircon U-Pb data for a host granodiorite (BJS12-04host) and a mafic magmatic enclave (BJS12-04MME).

Table 2: Microprobe analysis of plagioclase in the host granodiorites and the mafic magmatic enclaves.

Table 3: Microprobe analysis of amphibole in the host granodiorites and the mafic magmatic enclaves.

Table 4: Whole-rock major and trace element analyses of the host granodiorite and the mafic magmatic enclaves.

Table 5: Whole rock Sr-Nd-Hf isotopic compositions for the host granodiorite and the mafic magmatic

enclaves.

Table 6: Isotopic compositions of melts derived from two geochemical end-members.

Appendix：The Sr-Nd-Hf isotopes replicate analyses results of the international reference materials

Colour Figure
Click here to download Colour Figure: Figures revised.pdf

Fig.1

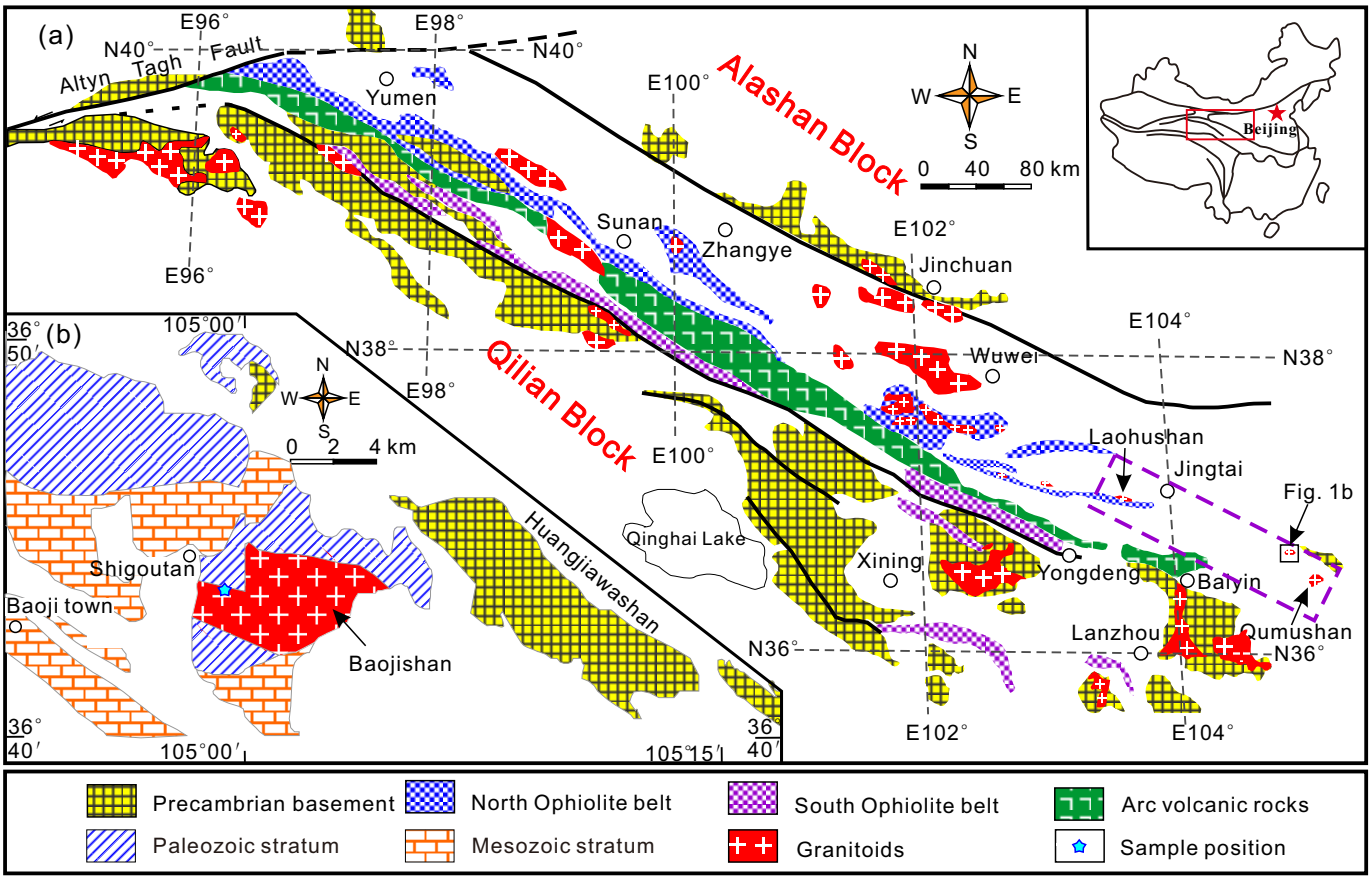

Fig. 2

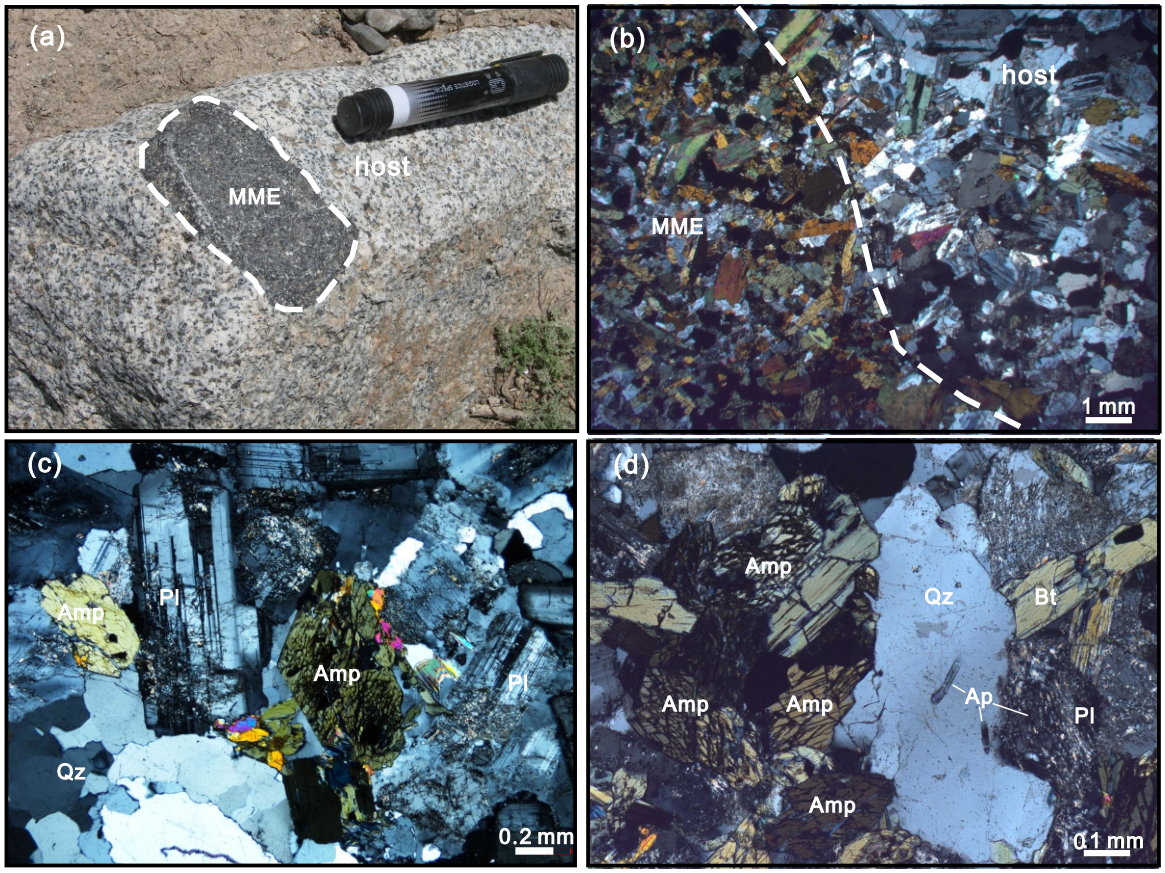
(a)
MME
host
(b)
host
MME
1 mm
(c)
Amp
Pl
Amp
Pl
Qz
0.2 mm
(d)
Amp
Qz
Bt
Amp
Amp
Ap
Pl
Amp
0.1 mm

Fig. 3


(a) BJS12-04host
Age (Ma)
100 μm
431.6±6.1
03
04
429.3±6.1
06
431.5±6.2
07
435.9±6.4
08
432.3±5.6
09
429.9±5.6
11
433.1±6.4
434.6±7.1
13
14
437.4±7.1
430.2±6.7
15
(b) BJS12-04MME
Age (Ma)
100 μm
3
431.2±4.9
4
432.9±4.8
426.6±5.1
5
7
431.0±4.7
8
437.6±5.0
10
433.6±6.0
11
433.8±5.2
12
431.9±5.4
14
429.1±4.7
15
428.7±5.1

Fig. 4

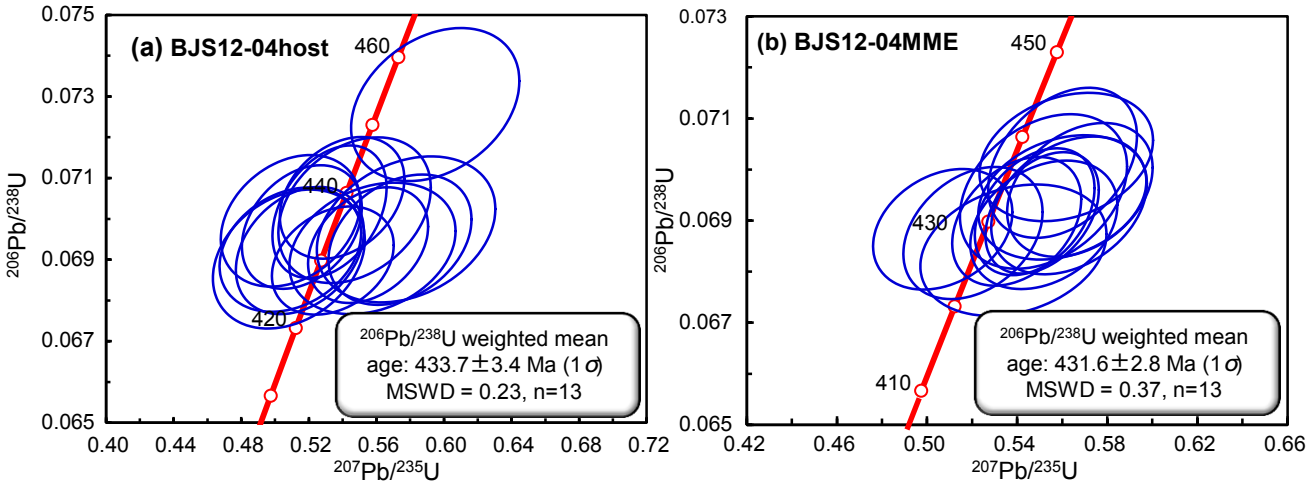
(a) BJS12-04host
460
440
420
$^{206}Pb/^{238}U$ weighted mean
age: 433.7±3.4 Ma (1σ)
MSWD = 0.23, n=13
$^{206}Pb/^{238}U$
$^{207}Pb/^{235}U$
0.075
0.073
0.071
0.069
0.067
0.065
0.40
0.44
0.48
0.52
0.56
0.60
0.64
0.68
0.72
(b) BJS12-04MME
450
430
410
$^{206}Pb/^{238}U$ weighted mean
age: 431.6±2.8 Ma (1σ)
MSWD = 0.37, n=13
$^{206}Pb/^{238}U$
$^{207}Pb/^{235}U$
0.073
0.071
0.069
0.067
0.065
0.42
0.46
0.50
0.54
0.58
0.62
0.66

Fig. 5

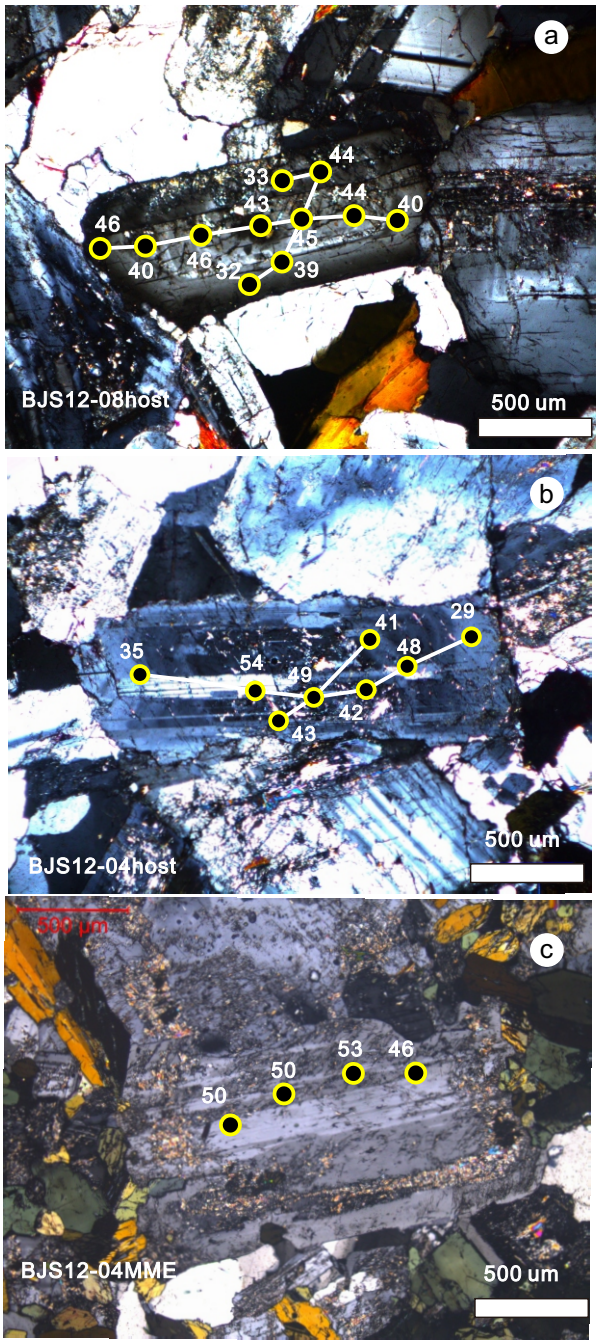
a
44
33
44
43
40
46
45
40
46
32
39
BJS12-08host
500 um
b
41
29
35
48
54
49
42
43
BJS12-04host
500 um
500 µm
c
53
46
50
50
BJS12-04MME
500 um

Fig. 6

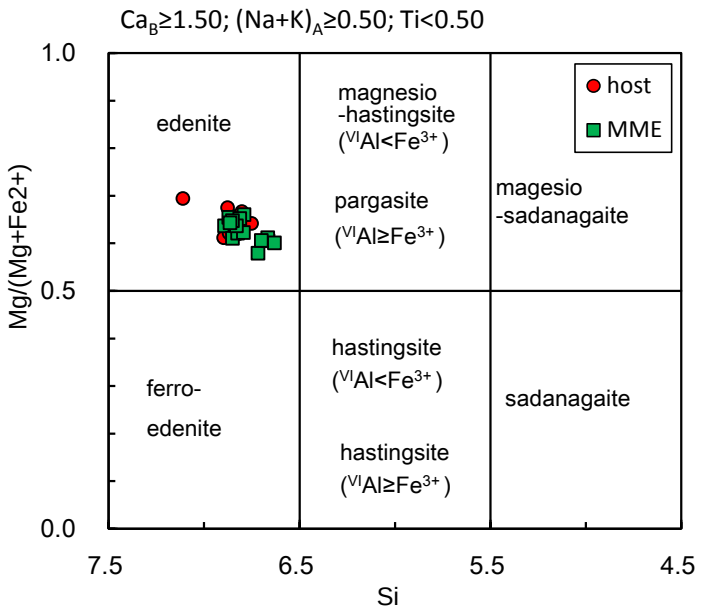
Ca_B≥1.50; $(Na+K)_A$≥0.50; Ti<0.50
1.0
0.5
0.0
Mg/(Mg+Fe2+)
7.5
6.5
5.5
4.5
Si
edenite
magnesio
-hastingsite
(^{VI}Al<Fe^{3+})
pargasite
(^{VI}Al≥Fe^{3+})
magesio
-sadanagaite
host
MME
ferro-
edenite
hastingsite
(^{VI}Al<Fe^{3+})
hastingsite
(^{VI}Al≥Fe^{3+})
sadanagaite

Fig . 7

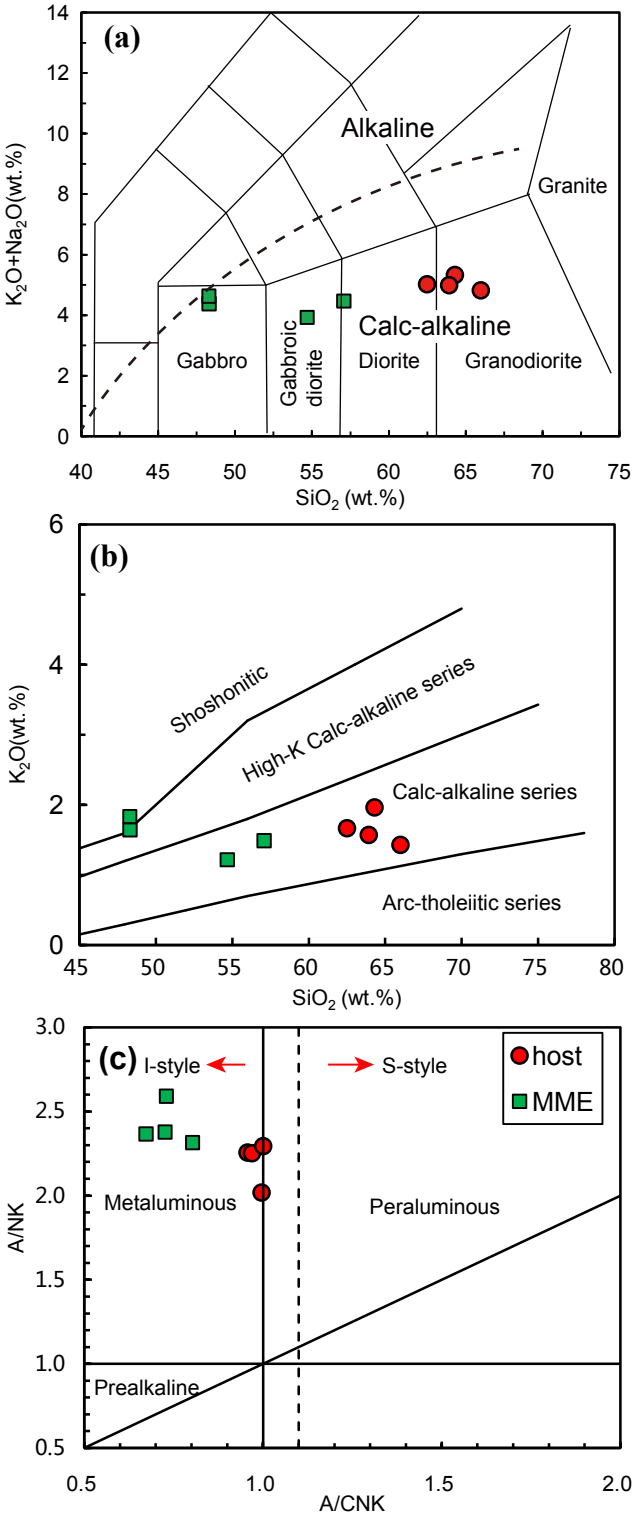
(a)
Alkaline
Granite
Calc-alkaline
Gabbro
Gabbroic diorite
Diorite
Granodiorite
K_2O+Na_2O(wt.%)
SiO_2 (wt.%)
(b)
Shoshonitic
High-K Calc-alkaline series
Calc-alkaline series
Arc-tholeiitic series
K_2O(wt.%)
SiO_2 (wt.%)
(c)
I-style
S-style
host
MME
Metaluminous
Peraluminous
Prealkaline
A/NK
A/CNK

Fig. 8

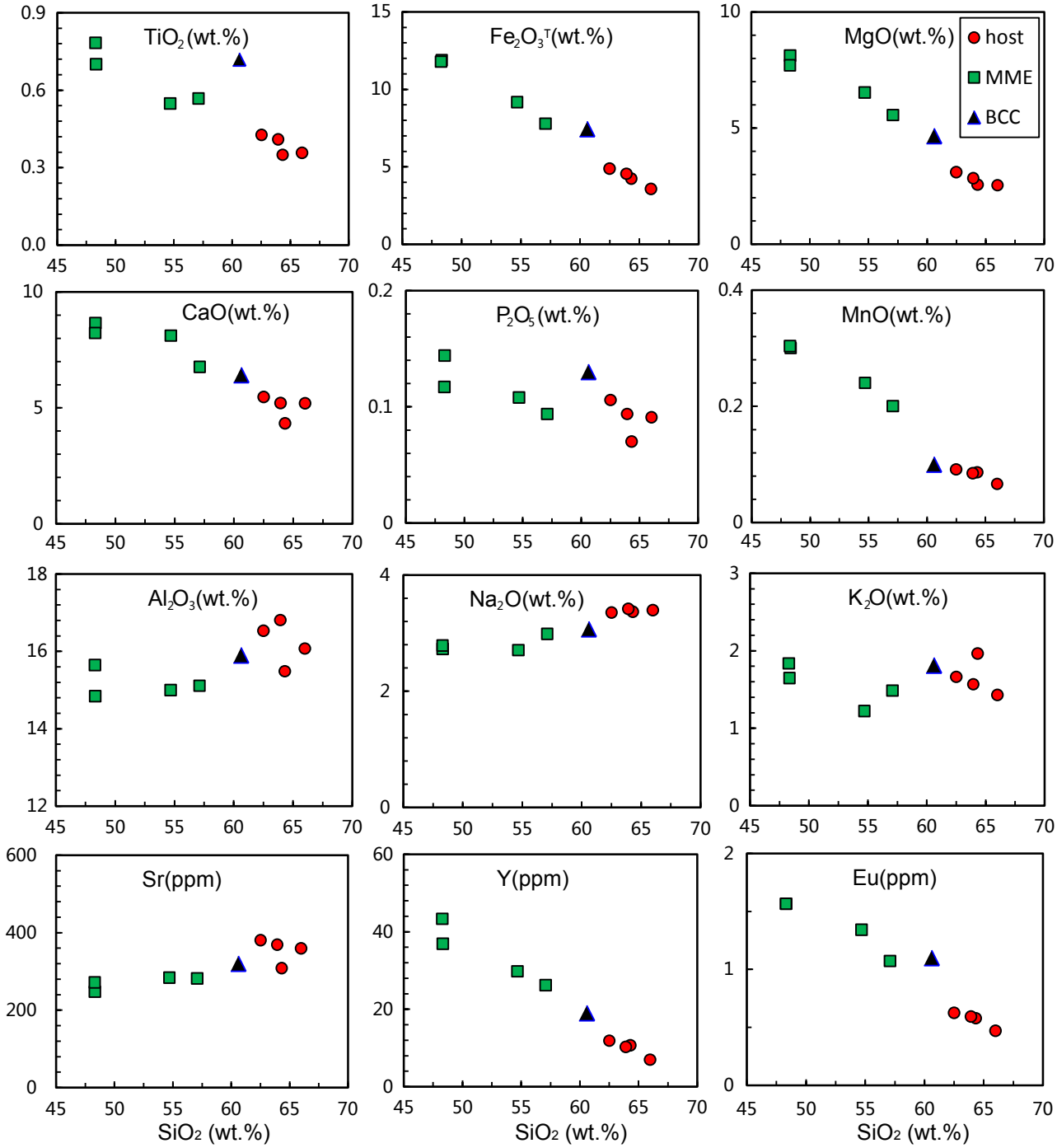
TiO2(wt.%)
Fe2O3T(wt.%)
MgO(wt.%)
host
MME
BCC
CaO(wt.%)
P2O5(wt.%)
MnO(wt.%)
Al2O3(wt.%)
Na2O(wt.%)
K2O(wt.%)
Sr(ppm)
Y(ppm)
Eu(ppm)
SiO2 (wt.%)
SiO2 (wt.%)
SiO2 (wt.%)

Fig. 9

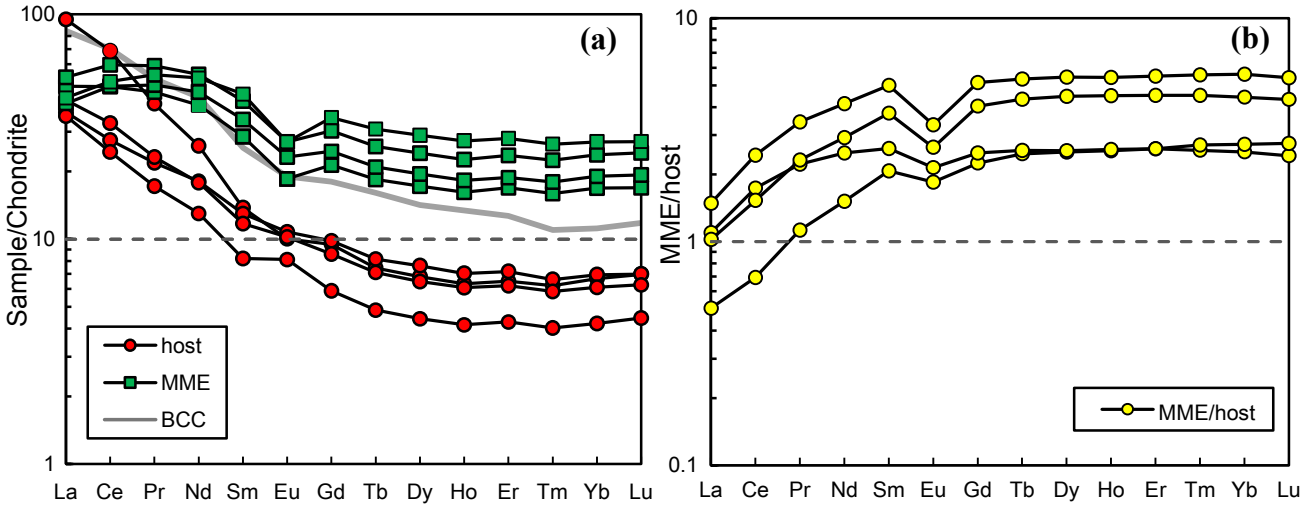
(a)
Sample/Chondrite
100
10
1
host
MME
BCC
La Ce Pr Nd Sm Eu Gd Tb Dy Ho Er Tm Yb Lu
(b)
MME/host
10
1
0.1
MME/host
La Ce Pr Nd Sm Eu Gd Tb Dy Ho Er Tm Yb Lu

Fig. 10

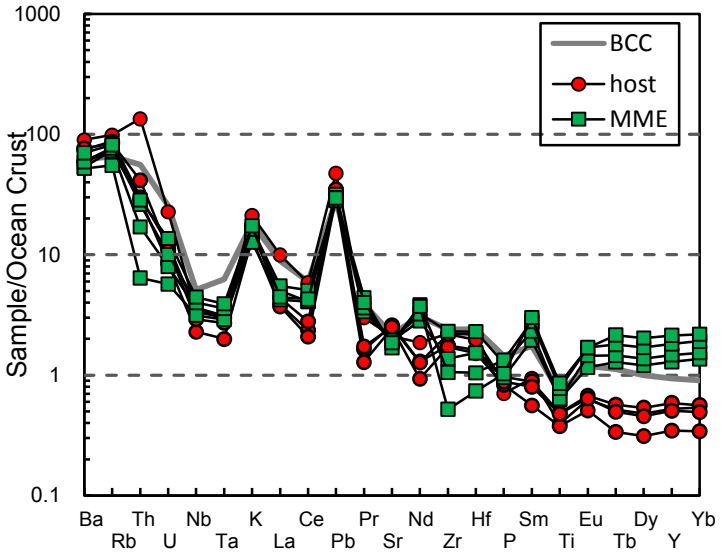
1000
100
10
1
0.1
Sample/Ocean Crust
BCC
host
MME
Ba
Rb
Th
U
Nb
Ta
K
La
Ce
Pb
Pr
Sr
Nd
Zr
Hf
P
Sm
Ti
Eu
Tb
Dy
Y
Yb

Fig. 11

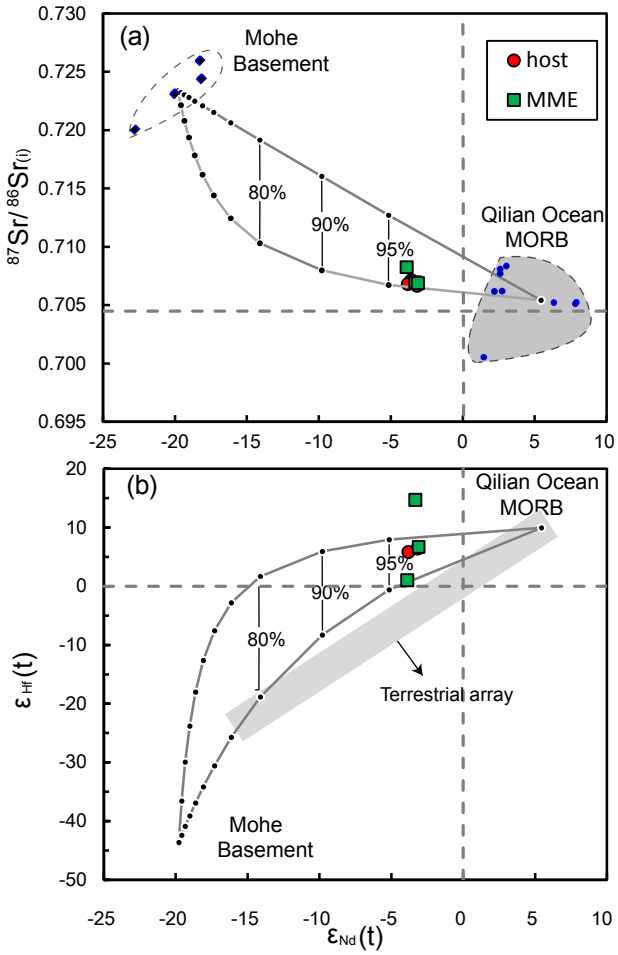
(a)
Mohe
Basement
host
MME
80%
90%
95%
Qilian Ocean
MORB
$^{87}Sr/^{86}Sr_{(i)}$
0.730
0.725
0.720
0.715
0.710
0.705
0.700
0.695
-25
-20
-15
-10
-5
0
5
10
(b)
Qilian Ocean
MORB
95%
90%
80%
Terrestrial array
Mohe
Basement
$\varepsilon_{Hf}(t)$
20
10
0
-10
-20
-30
-40
-50
$\varepsilon_{Nd}(t)$

Fig. 12

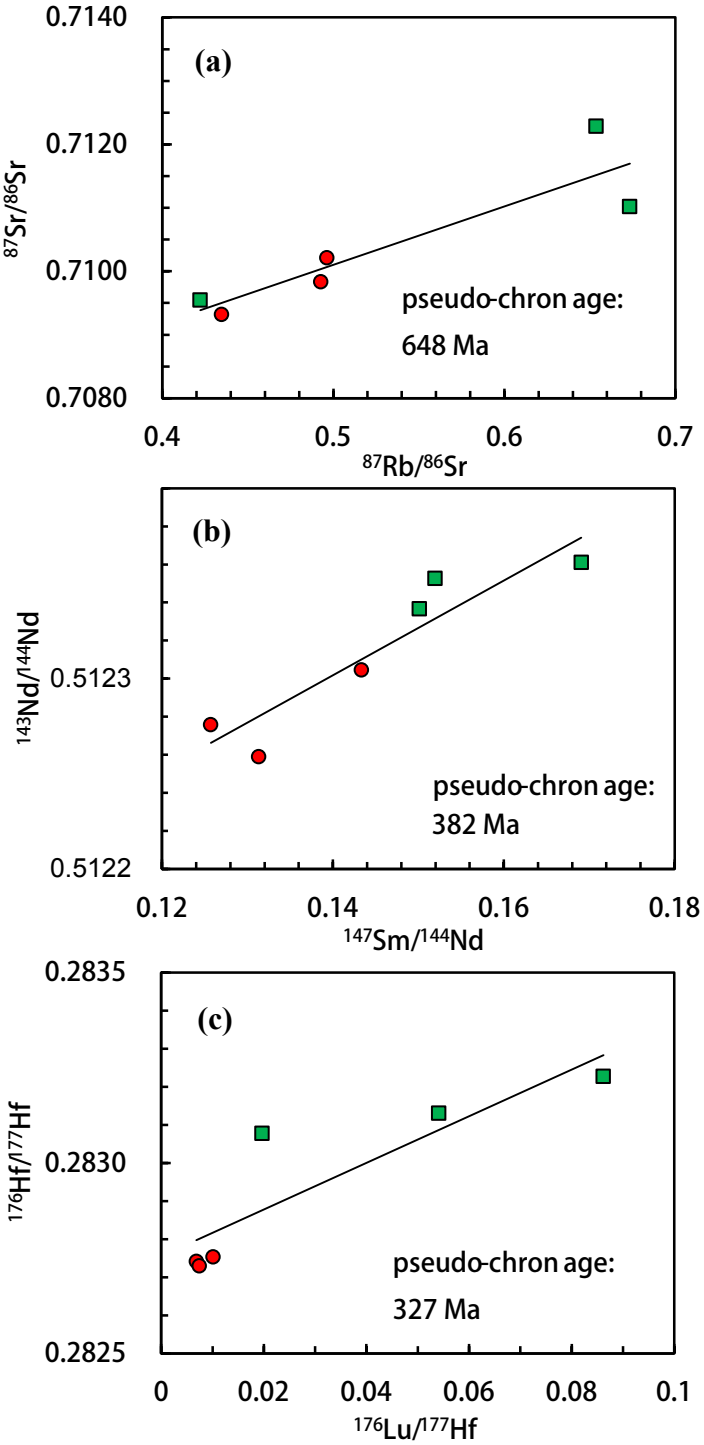
(a)
0.7140
0.7120
0.7100
0.7080
$^{87}Sr/^{86}Sr$
pseudo-chron age:
648 Ma
0.4
0.5
0.6
0.7
$^{87}Rb/^{86}Sr$
(b)
$^{143}Nd/^{144}Nd$
0.5123
0.5122
pseudo-chron age:
382 Ma
0.12
0.14
0.16
0.18
$^{147}Sm/^{144}Nd$
(c)
0.2835
0.2830
0.2825
$^{176}Hf/^{177}Hf$
pseudo-chron age:
327 Ma
0
0.02
0.04
0.06
0.08
0.1
$^{176}Lu/^{177}Hf$

Fig. 13

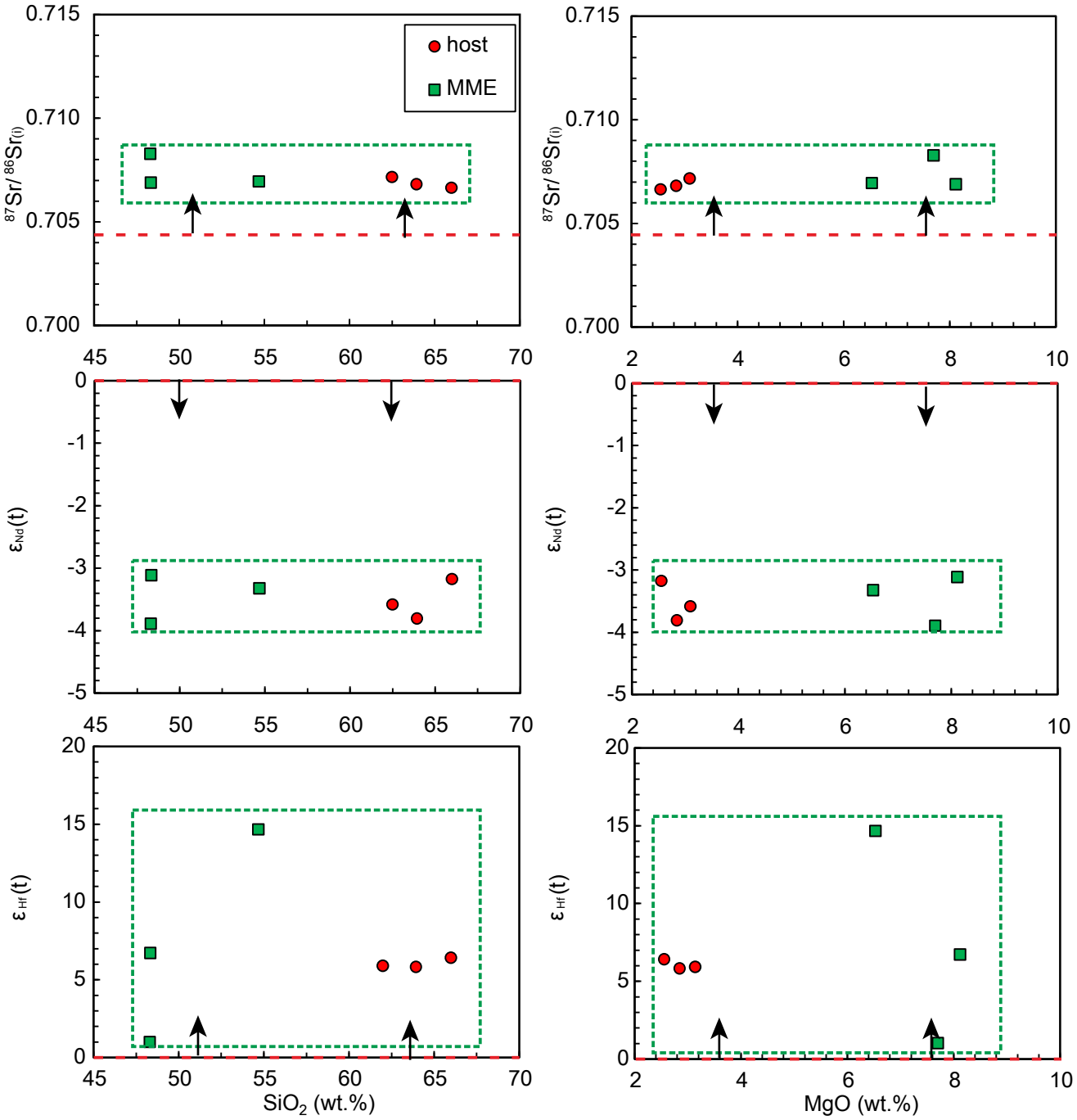
host
MME
$^{87}Sr/^{86}Sr_{(i)}$
$\varepsilon_{Nd}(t)$
$\varepsilon_{Hf}(t)$
SiO_2 (wt.%)
MgO (wt.%)

Fig. 14

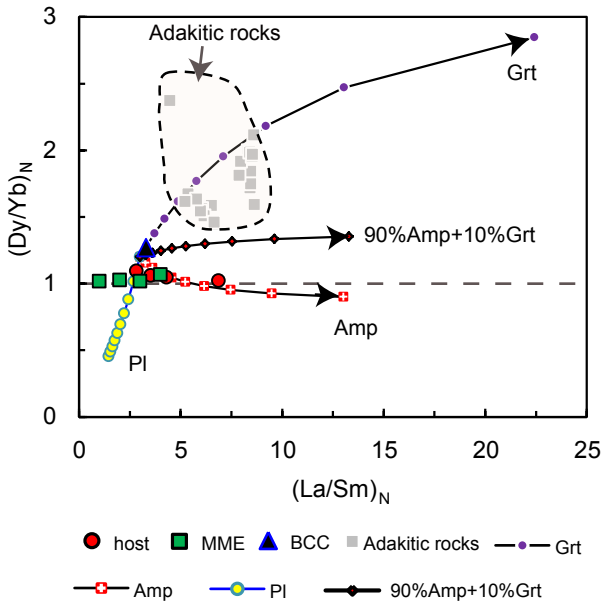
Adakitic rocks
Grt
90%Amp+10%Grt
Amp
Pl
(Dy/Yb)N
(La/Sm)N
0
1
2
3
0
5
10
15
20
25
host
MME
BCC
Adakitic rocks
Grt
Amp
Pl
90%Amp+10%Grt

Table

Click here to download Table: Table revised.pdf

Table 1: LA-ICP-MS zircon U-Pb data for a host granodiorite (BJS12-04host) and a mafic magmatic enclave (BJS12-04MME).

Spot	Concentrations (ppm)				Ratios						Age (Ma)					
	Pb	Th	U	Th/U	$^{207}Pb/^{206}Pb$	1σ	$^{207}Pb/^{235}U$	1σ	$^{206}Pb/^{238}U$	1σ	$^{207}Pb/^{206}Pb$	1σ	$^{207}Pb/^{235}U$	1σ	$^{206}Pb/^{238}U$	1σ
host (BJS12-04host)																
01	20.63	60.13	185.6	0.3	0.0531	0.0024	0.5159	0.0234	0.0698	0.0010	331.5	101.8	422.4	15.7	434.9	6.0
02	19.75	58.08	174.6	0.3	0.0552	0.0024	0.5323	0.0223	0.0702	0.0011	420.4	99.1	433.3	14.8	437.2	6.5
03	17.04	53.56	137.0	0.4	0.0532	0.0028	0.5091	0.0277	0.0692	0.0010	338.9	120.4	417.8	18.6	431.6	6.1
04	32.07	111.5	202.6	0.6	0.0557	0.0026	0.5397	0.0243	0.0705	0.0010	438.9	97.2	438.2	16.0	439.3	5.9
05	25.32	75.89	136.9	0.6	0.0632	0.0037	0.6326	0.0372	0.0730	0.0012	716.7	124.1	497.7	23.1	454.2	7.1
06	21.65	62.47	170.2	0.4	0.0540	0.0026	0.5147	0.0250	0.0692	0.0010	372.3	107.4	421.6	16.8	431.5	6.2
07	20.14	58.92	165.8	0.4	0.0527	0.0027	0.5092	0.0272	0.0700	0.0011	316.7	116.7	417.9	18.3	435.9	6.4
08	21.76	67.04	188.1	0.4	0.0581	0.0026	0.5551	0.0234	0.0694	0.0009	600.0	96.3	448.3	15.3	432.3	5.6
09	20.47	66.65	148.4	0.4	0.0558	0.0025	0.5342	0.0238	0.0690	0.0009	442.6	98.1	434.6	15.7	430.0	5.3
10	21.47	78.73	134.1	0.6	0.0586	0.0035	0.5577	0.0325	0.0693	0.0011	550.0	133.3	450.0	21.2	431.8	6.4
11	23.82	72.93	183.1	0.4	0.0594	0.0029	0.5740	0.0279	0.0695	0.0011	588.9	102.8	460.6	18.0	433.1	6.4
12	15.57	43.40	128.4	0.3	0.0601	0.0034	0.5949	0.0329	0.0728	0.0012	609.3	123.0	474.0	20.9	453.0	7.4
13	16.39	56.52	118.4	0.5	0.0601	0.0036	0.5776	0.0349	0.0697	0.0012	605.6	129.6	462.9	22.5	434.6	7.1
14	17.68	53.54	138.5	0.4	0.0569	0.0032	0.5471	0.0298	0.0702	0.0012	487.1	119.4	443.1	19.5	437.4	7.1
15	11.80	36.10	94.73	0.4	0.0540	0.0032	0.5082	0.0297	0.0690	0.0011	368.6	135.2	417.2	20.0	430.2	6.8
MME (BJS12-04MME)																
01	27.73	82.33	207.9	0.4	0.0582	0.0023	0.5602	0.0218	0.0701	0.0010	600.0	85.2	451.6	14.2	436.9	5.8
02	40.73	138.6	281.4	0.5	0.0570	0.0021	0.5398	0.0189	0.0690	0.0008	500.0	79.6	438.3	12.5	430.0	5.0
03	62.18	227.8	323.5	0.7	0.0578	0.0020	0.5478	0.0175	0.0692	0.0008	524.1	69.4	443.5	11.5	431.2	4.9
04	34.01	109.9	226.7	0.5	0.0589	0.0026	0.5601	0.0246	0.0695	0.0008	561.1	98.1	451.6	16.0	432.9	4.8
05	23.13	73.40	173.0	0.4	0.0573	0.0030	0.5384	0.0273	0.0684	0.0008	501.9	114.8	437.3	18.0	426.6	5.1
06	28.94	90.91	223.2	0.4	0.0578	0.0022	0.5518	0.0215	0.0689	0.0008	520.4	88.0	446.2	14.1	429.6	5.0
07	59.26	215.4	314.9	0.7	0.0578	0.0018	0.5511	0.0166	0.0692	0.0008	520.4	68.5	445.7	10.9	431.0	4.7
08	34.18	112.9	204.9	0.6	0.0575	0.0026	0.5618	0.0254	0.0702	0.0008	509.3	98.1	452.7	16.5	437.6	5.0
09	28.07	80.18	223.6	0.4	0.0621	0.0026	0.6018	0.0260	0.0700	0.0010	677.5	90.7	478.4	16.5	436.2	5.9
10	31.98	102.2	211.0	0.5	0.0574	0.0026	0.5517	0.0245	0.0696	0.0010	509.3	98.9	446.1	16.0	433.6	6.0
11	51.94	175.3	369.7	0.5	0.0586	0.0021	0.5679	0.0213	0.0696	0.0009	550.0	75.0	456.6	13.8	433.8	5.2
12	36.00	106.1	330.1	0.3	0.0583	0.0022	0.5630	0.0228	0.0693	0.0009	542.6	89.8	453.5	14.8	431.9	5.4
13	24.74	80.67	187.6	0.4	0.0617	0.0032	0.5952	0.0316	0.0695	0.0010	664.8	112.9	474.2	20.1	433.4	6.3
14	39.00	137.7	253.1	0.5	0.0530	0.0022	0.5070	0.0204	0.0688	0.0008	331.5	92.6	416.4	13.8	429.1	4.7
15	37.30	135.2	246.0	0.5	0.0548	0.0022	0.5204	0.0204	0.0688	0.0009	405.6	86.1	425.4	13.6	428.7	5.1

Table 2: Microprobe analysis of plagioclase in the host granodiorites and the mafic magmatic enclaves.

Spot	SiO_2	Al_2O_3	CaO	Na_2O	K_2O	Total	Si	Al	Ca	Na	K	Sum	An
host (BJS12-08host) Fig. 5 (a)													
1.1	56.2	27.4	9.5	6.1	0.07	99.4	2.57	1.41	0.47	0.54	0.00	5.00	46
1.2	57.5	26.2	8.4	6.9	0.24	99.4	2.63	1.34	0.41	0.61	0.01	5.01	40
1.3	56.8	27.1	9.5	6.2	0.17	99.8	2.59	1.38	0.47	0.55	0.01	5.00	46
1.4	56.6	26.6	9.1	6.5	0.12	99.0	2.60	1.37	0.45	0.58	0.01	5.00	43
1.5	56.4	27.2	9.6	6.3	0.12	99.7	2.58	1.40	0.47	0.56	0.01	5.01	45
1.6	56.8	27.2	9.2	6.5	0.07	99.9	2.59	1.39	0.45	0.57	0.00	5.01	44
1.7	56.2	25.1	7.9	6.5	0.05	95.8	2.65	1.33	0.40	0.59	0.00	4.98	40
1.8	60.1	25.1	6.9	7.9	0.20	100.5	2.71	1.27	0.33	0.69	0.01	5.01	32
1.9	58.1	26.0	8.2	7.1	0.20	99.8	2.64	1.33	0.40	0.63	0.01	5.01	39
1.1	60.2	25.7	6.9	7.7	0.14	100.8	2.70	1.29	0.33	0.66	0.01	4.99	33
1.11	57.2	26.6	9.1	6.2	0.14	99.4	2.61	1.36	0.45	0.55	0.01	4.98	44
host (BJS12-04host) Fig. 5 (b)													
1.1	58.6	25.7	7.5	7.6	0.30	99.8	2.66	1.31	0.36	0.67	0.02	5.02	35
1.2	53.9	28.7	11.5	5.2	0.24	99.7	2.49	1.48	0.57	0.46	0.01	5.01	54
1.3	55.1	27.7	10.5	5.8	0.22	99.7	2.54	1.43	0.52	0.52	0.01	5.01	49
1.4	57.9	26.5	8.5	6.5	0.22	99.8	2.63	1.35	0.42	0.57	0.01	4.98	42
1.5	55.7	27.9	10.2	5.9	0.20	100.2	2.54	1.43	0.50	0.52	0.01	5.01	48
1.6	60.8	24.8	6.3	8.3	0.12	100.4	2.73	1.25	0.30	0.72	0.01	5.01	29
1.7	54.6	28.1	11.0	5.6	0.16	99.6	2.51	1.45	0.54	0.49	0.01	5.01	52
1.8	56.9	27.1	9.2	6.5	0.21	100.1	2.59	1.38	0.45	0.57	0.01	5.01	43
1.9	57.4	26.6	8.7	6.8	0.16	99.8	2.61	1.36	0.42	0.60	0.01	5.01	41
MME (BJS12-04MME) Fig. 5 (c)													
1.1	55.0	27.4	10.4	5.7	0.08	98.8	2.55	1.42	0.51	0.51	0.00	5.00	50
1.2	54.6	27.8	10.3	5.5	0.12	98.5	2.53	1.45	0.51	0.50	0.01	5.00	50
1.3	54.5	28.5	11.1	5.4	0.13	99.9	2.50	1.47	0.55	0.48	0.01	5.01	53
2.4	56.2	27.5	9.7	6.3	0.11	100.0	2.56	1.41	0.48	0.56	0.01	5.01	46
2.1	55.7	27.3	9.4	6.4	0.30	99.5	2.56	1.41	0.46	0.57	0.02	5.03	44
2.2	57.3	26.8	8.9	6.9	0.12	100.2	2.60	1.37	0.43	0.61	0.01	5.02	41
3.1	59.5	24.9	7.0	7.8	0.17	99.6	2.70	1.27	0.34	0.69	0.01	5.01	33
3.2	58.1	26.2	8.4	7.2	0.18	100.2	2.64	1.33	0.41	0.63	0.01	5.02	39
3.3	61.5	24.2	5.7	8.3	0.29	100.2	2.76	1.22	0.27	0.72	0.02	5.00	27
MME (BJS12-08MME)													
1.1	56.8	26.6	8.8	6.7	0.16	99.3	2.60	1.37	0.43	0.59	0.01	5.01	42
1.2	58.6	25.7	8.0	7.3	0.17	99.9	2.66	1.31	0.39	0.64	0.01	5.01	37
1.3	55.5	28.0	9.1	5.3	1.23	99.5	2.56	1.45	0.45	0.48	0.07	5.00	45
2.1	60.6	24.5	6.1	8.5	0.13	100.1	2.74	1.24	0.29	0.75	0.01	5.02	28
3.1	55.6	27.9	10.2	5.9	0.14	99.9	2.54	1.43	0.50	0.52	0.01	5.00	49
4.1	56.2	27.5	9.7	6.0	0.27	99.8	2.57	1.41	0.48	0.53	0.02	5.00	47

Structural formulas on the basis of 8 oxygen atoms

Table 3: Microprobe analysis of amphibole in the host granodiorites and the mafic magmatic enclaves

Spot	SiO_2	TiO_2	Al_2O_3	Cr_2O_3	FeO^T	MnO	MgO	CaO	Na_2O	K_2O	Total	Si	Ti	AlI^V	Al^{VI}	Cr	Fe^{3+}	Fe^{2+}	Mn	Mg	Ca	Na	K	Sum	Mg#
host (BJS12-04host)																									
1.1	46.9	0.60	7.9	0.04	15.8	0.58	12.8	11.6	1.16	0.76	98.09	6.87	0.07	1.13	0.22	0.00	0.50	1.44	0.07	2.79	1.82	0.33	0.14	16.73	0.66
2.1	46.3	0.58	8.1	0.08	16.1	0.56	11.8	11.4	1.29	0.69	96.84	6.90	0.06	1.10	0.32	0.01	0.34	1.67	0.07	2.62	1.82	0.37	0.13	16.83	0.61
2.2	46.2	0.65	8.3	0.08	15.8	0.61	11.9	11.5	1.29	0.61	96.92	6.87	0.07	1.13	0.33	0.01	0.35	1.61	0.08	2.64	1.82	0.37	0.12	16.85	0.62
2.3	46.3	0.67	8.7	0.01	16.1	0.70	11.9	11.4	1.49	0.55	97.90	6.82	0.07	1.18	0.33	0.00	0.38	1.60	0.09	2.61	1.80	0.43	0.10	16.94	0.62
host (BJS12-08host)																									
1.1	46.5	1.08	8.6	0.12	14.6	0.48	12.7	11.6	1.38	0.43	97.43	6.83	0.12	1.17	0.31	0.01	0.33	1.46	0.06	2.79	1.82	0.39	0.08	16.86	0.66
1.2	47.0	0.57	8.0	0.05	15.0	0.53	13.2	11.6	1.38	0.52	97.80	6.88	0.06	1.12	0.25	0.01	0.44	1.38	0.07	2.87	1.82	0.39	0.10	16.77	0.67
2.1	46.2	0.69	8.9	0.02	14.4	0.59	12.8	11.7	1.45	0.40	97.10	6.80	0.08	1.20	0.35	0.00	0.37	1.40	0.07	2.80	1.84	0.41	0.08	16.95	0.67
2.2	45.5	1.13	8.9	0.02	14.9	0.42	12.3	11.7	1.41	0.58	97.01	6.75	0.13	1.25	0.31	0.00	0.33	1.52	0.05	2.73	1.86	0.40	0.11	16.99	0.64
2.3	46.5	0.67	8.7	0.06	14.7	0.50	12.5	11.8	1.18	0.48	97.13	6.85	0.07	1.15	0.36	0.01	0.35	1.46	0.06	2.75	1.87	0.34	0.09	16.86	0.65
3.1	46.2	0.67	8.8	0.04	15.2	0.44	12.5	11.9	1.17	0.46	97.44	6.79	0.07	1.21	0.31	0.00	0.46	1.41	0.05	2.74	1.87	0.33	0.09	16.87	0.66
4.1	44.9	1.08	9.5	0.13	16.2	0.67	11.0	11.2	1.72	0.60	96.93	6.72	0.12	1.28	0.39	0.02	0.23	1.79	0.08	2.46	1.80	0.50	0.11	17.18	0.58
4.2	44.9	1.08	9.5	0.10	16.2	0.64	11.4	11.7	1.52	0.57	97.60	6.66	0.12	1.34	0.32	0.01	0.37	1.64	0.08	2.52	1.85	0.44	0.11	17.13	0.61
4.3	45.1	1.10	9.4	0.06	16.3	0.57	11.6	11.5	1.64	0.56	97.94	6.67	0.12	1.33	0.30	0.01	0.39	1.63	0.07	2.56	1.82	0.47	0.11	17.12	0.61
MME (BJS12-04MME)																									
1.1	47.1	1.24	8.2	0.11	14.8	0.75	12.6	11.1	1.61	0.47	97.99	6.89	0.14	1.11	0.30	0.01	0.24	1.57	0.09	2.76	1.75	0.46	0.09	16.82	0.64
1.2	46.1	0.69	8.5	0.09	15.7	0.60	12.1	11.3	1.43	0.69	97.17	6.84	0.08	1.16	0.32	0.01	0.36	1.59	0.08	2.67	1.80	0.41	0.13	16.91	0.63
1.3	45.0	1.45	9.4	0.14	15.1	0.64	11.7	11.4	1.65	0.74	97.15	6.70	0.16	1.30	0.35	0.02	0.19	1.69	0.08	2.59	1.81	0.48	0.14	17.17	0.61
2.1	44.3	1.36	9.8	0.08	16.0	0.64	11.2	11.1	1.63	0.70	96.85	6.63	0.15	1.37	0.36	0.01	0.34	1.67	0.08	2.51	1.77	0.47	0.13	17.21	0.60
2.2	46.0	0.60	8.4	0.05	16.3	0.54	11.6	11.6	1.18	0.68	96.89	6.85	0.07	1.15	0.32	0.01	0.38	1.65	0.07	2.58	1.85	0.34	0.13	16.86	0.61
MME (BJS12-08MME)																									
1.1	46.8	0.81	9.1	0.02	14.5	0.67	12.7	10.3	1.92	0.26	97.04	6.87	0.09	1.13	0.45	0.00	0.31	1.47	0.08	2.78	1.62	0.55	0.05	16.97	0.65
1.2	45.4	0.66	8.6	0.02	14.9	0.49	12.0	11.9	1.18	0.56	95.71	6.81	0.07	1.19	0.34	0.00	0.34	1.54	0.06	2.68	1.91	0.34	0.11	16.93	0.64
1.3	45.7	0.67	8.7	0.07	15.2	0.48	11.9	11.9	1.28	0.58	96.43	6.82	0.07	1.18	0.35	0.01	0.28	1.62	0.06	2.65	1.91	0.37	0.11	16.96	0.62
2.1	46.3	0.73	9.1	0.07	14.9	0.57	12.3	11.4	1.25	0.46	97.20	6.81	0.08	1.19	0.40	0.01	0.39	1.44	0.07	2.70	1.80	0.36	0.09	16.92	0.65
2.2	45.7	0.72	9.0	0.15	15.4	0.55	11.9	11.5	1.62	0.37	96.84	6.79	0.08	1.21	0.36	0.02	0.31	1.60	0.07	2.64	1.83	0.47	0.07	17.01	0.62
2.3	46.2	0.66	8.8	0.13	15.2	0.59	12.1	11.5	1.36	0.43	96.96	6.83	0.07	1.17	0.37	0.01	0.36	1.52	0.07	2.67	1.82	0.39	0.08	16.91	0.64
3.1	46.3	0.71	8.6	0.07	15.1	0.56	12.3	11.4	1.16	0.58	96.88	6.85	0.08	1.15	0.35	0.01	0.39	1.48	0.07	2.71	1.81	0.33	0.11	16.84	0.65
3.2	46.5	1.10	8.5	0.02	15.0	0.61	12.4	11.0	1.53	0.28	96.92	6.86	0.12	1.14	0.34	0.00	0.33	1.52	0.08	2.73	1.74	0.44	0.05	16.83	0.64

Structural formulas on the basis of 23 oxygen atoms; Mg# =Mg/(Mg +Fe^{2+})(molar ratio).

Table 4: Whole-rock major and trace element analyses of the host granodiorite and the mafic magmatic enclaves.

Type	host				MME			
Sample	BJS12-04host	BJS12-06host	BJS12-08host	BJS12-10host	BJS12-04MME	BJS12-06MME	BJS12-08MME	BJS12-10MME
SiO_2	64.3	62.5	66.0	63.9	57.1	54.7	48.3	48.3
TiO_2	0.35	0.43	0.36	0.41	0.57	0.55	0.70	0.78
Al_2O_3	15.5	16.5	16.1	16.8	15.1	15.0	14.8	15.6
$Fe_2O_3^T$	4.23	4.88	3.58	4.57	7.80	9.17	11.88	11.81
MnO	0.09	0.09	0.07	0.09	0.20	0.24	0.30	0.30
MgO	2.58	3.10	2.55	2.84	5.57	6.53	8.12	7.70
CaO	4.33	5.47	5.19	5.21	6.76	8.12	8.67	8.24
Na_2O	3.37	3.36	3.40	3.42	2.99	2.71	2.73	2.79
K_2O	1.96	1.67	1.43	1.57	1.49	1.22	1.65	1.84
P_2O_5	0.07	0.11	0.09	0.09	0.09	0.11	0.14	0.12
L[illegible]	1.13	1.13	1.04	1.16	1.26	0.94	1.05	1.38
Total	97.9	99.3	99.8	100.1	98.9	99.3	98.4	98.9
$Mg^{\#}$	0.55	0.56	0.59	0.56	0.59	0.59	0.58	0.57
A/NK	1.00	0.96	0.97	1.00	0.80	0.73	0.67	0.73
A/CNK	2.02	2.26	2.25	2.29	2.32	2.59	2.37	2.38
Na_2O/K_2O	1.72	2.01	2.38	2.18	2.01	2.22	1.66	1.52
Sc	12.0	14.0	8.6	11.7	30.8	31.4	43.6	50.5
V	88.1	99.6	61.2	92.8	162	177	239	253
Cr	68.9	92.8	64.3	83.2	269	409	547	354
Ni	23.9	26.1	28.5	22.5	49.4	100.2	116.2	68.0
Rb	73.8	65.2	54.0	62.8	54.9	41.4	57.7	61.3
Sr	308	380	359	369	282	284	248	271
Y	10.7	11.9	7.0	10.3	26.2	29.8	36.9	43.4
Zr	122	97.9	94.7	121	75.9	128	58.6	28.8
Nb	5.34	5.30	3.59	4.58	5.72	4.94	6.29	6.99
Cs	2.78	2.91	2.07	2.89	1.79	2.43	3.34	2.58
Ba	666	548	439	566	397	385	438	520
La	22.5	8.7	8.4	9.8	11.3	9.5	12.4	10.1
Ce	42.0	16.9	14.9	20.1	29.1	29.3	36.4	30.7
Pr	3.80	2.07	1.63	2.20	4.28	4.61	5.60	5.11
Nd	12.1	8.45	6.07	8.33	18.4	21.1	25.2	24.3
Sm	2.11	1.99	1.25	1.80	4.37	5.20	6.28	6.75
Eu	0.58	0.63	0.47	0.59	1.07	1.34	1.57	1.57
Gd	1.95	2.02	1.21	1.77	4.38	5.05	6.24	7.13
Tb	0.28	0.31	0.18	0.27	0.69	0.78	0.97	1.15
Dy	1.73	1.94	1.12	1.65	4.36	4.95	6.13	7.35
Ho	0.36	0.40	0.24	0.34	0.92	1.03	1.28	1.55
Er	1.08	1.19	0.71	1.03	2.80	3.10	3.91	4.64
Tm	0.16	0.17	0.10	0.15	0.41	0.46	0.57	0.67
Yb	1.13	1.18	0.72	1.04	2.87	3.23	4.03	4.61
Lu	0.18	0.18	0.11	0.16	0.43	0.49	0.61	0.69
Hf	3.33	2.49	2.34	3.04	2.35	3.53	1.61	1.13
Ta	0.35	0.34	0.22	0.30	0.35	0.32	0.40	0.44
Pb	18.6	12.3	11.5	13.7	12.4	11.6	11.0	11.6
Th	13.5	3.01	2.85	4.15	1.70	0.64	2.62	2.85
U	1.16	0.62	0.43	0.56	0.41	0.29	0.51	0.70
Nb/Ta	15.2	15.8	16.1	15.1	16.4	15.2	15.7	15.9

$Mg^{\#}=Mg^{2+}/(Mg^{2+}+Fe^{2+})$(molar ratio);

A/CNK= $Al_2O_3/(CaO+Na_2O+K_2O)$ (molar ratio); A/NK= $Al_2O_3/(Na_2O+K_2O)$ (molar ratio).

Table 5: Whole rock Sr-Nd-Hf isotopic composition for the host granodiorite and the mafic magmatic enclaves[a].

Sample	Rb	Sr	$^{87}Sr/^{86}Sr$		$^{87}Sr/^{86}Sr_{(i)}$[b]	Sm	Nd	$^{143}Nd/^{144}Nd$		$^{143}Nd/^{144}Nd_{(i)}$[c]	$\varepsilon_{Nd}(t)$[c]	Lu	Hf	$^{176}Hf/^{177}Hf$		$^{176}Hf/^{177}Hf_{(i)}$[d]	$\varepsilon_{Hf}(t)$[d]
	(ppm)	(ppm)	ratio	$\pm 2\sigma$		(ppm)	(ppm)	ratio	$\pm 2\sigma$			(ppm)	(ppm)	ratio	$\pm 2\sigma$		
BJS12-06host	65.2	380.4	0.710213	10	0.707173	2.0	8.4	0.512305	5	0.511901	-3.6	0.18	2.49	0.282753	6	0.282672	5.9
BJS12-08host	54.0	359.3	0.709318	10	0.706656	1.3	6.1	0.512276	6	0.511922	-3.2	0.11	2.34	0.282741	4	0.282686	6.4
BJS12-10host	62.8	368.8	0.709831	8	0.706814	1.8	8.3	0.512259	6	0.511889	-3.8	0.16	3.04	0.282729	4	0.282669	5.8
BJS12-06MME	41.4	283.8	0.709547	14	0.706961	5.2	21.1	0.512337	8	0.511914	-3.3	0.49	3.53	0.283078	5	0.282919	14.7
BJS12-08MME	57.7	248.0	0.711017	14	0.706893	6.3	25.2	0.512353	7	0.511925	-3.1	0.61	1.61	0.283130	5	0.282695	6.7
BJS12-10MME	61.3	271.5	0.712283	10	0.708280	6.8	24.3	0.512361	5	0.511885	-3.9	0.69	1.13	0.283227	5	0.282533	1.0

a. See text for analytical details.

b. $^{87}Sr/^{86}Sr_{(i)}=[(^{87}Sr/^{86}Sr)-(^{87}Rb/^{86}Sr)(e^{\lambda t}-1)]$, where λ (^{87}Rb)=1.42×10^{-11}, t=430Ma.

c. $^{143}Nd/^{144}Nd_{(i)}=[(^{143}Nd/^{144}Nd)-(^{143}Sm/^{144}Nd)(e^{\lambda t}-1)]$, $\varepsilon_{Nd}(t)=[(^{143}Nd/^{144}Nd)/(^{143}Nd/^{144}Nd_{CHUR})-1]$x10000, where λ (^{147}Sm)=6.54×10^{-12}, $^{143}Nd/^{144}Nd_{CHUR}$= 0.512638.

d. $^{176}Hf/^{177}Hf_{(i)}=[(^{176}Hf/^{177}Hf)-(^{176}Lu/^{177}Hf)(e^{\lambda t}-1)]$,$\varepsilon_{Hf}(t)=[(^{176}Hf/^{177}Hf)/(^{176}Hf/^{177}Hf_{CHUR})-1]$x10000, where λ (^{176}Lu)=1.93×10^{-11}, $^{176}Hf/^{177}Hf_{CHUR}$ = 0.282772.

Table 6: Isotopic compositions of melts derived from three geochemical end-members

Geochemical end-members	Mohe basement	North Qilian Ocean MORB	
		MAX	MIN
Rb(ppm)	145.3	44.02	0.44
Sr(ppm)	586.1	389.8	44.9
$^{87}Sr/^{86}Sr$	0.7279	0.7091	0.7051
Sm(ppm)	5.8	6.81	0.89
Nd(ppm)	33.0	27.11	2.39
$^{143}Nd/^{144}Nd$	0.5114	0.5131	0.5126
Lu(ppm)	0.24	0.71	0.19
Hf(ppm)	0.4	4.72	0.74
$^{176}Hf/^{177}Hf$	0.2814		

The concentration of Rb, Sr, Sm, Lu and Hf, together with Sr-Nd-Hf isotopic values for Mohe basement are averages based on Chen et al. (2007) and Li et al. (2007). The concentration of Rb, Sr, Sm, Lu and Hf, together with Sr-Nd isotopic values for North Qilian Ocean MORB are from Hou et al. (2006a, 2006b).Hf isotope for MORB is inferred from Nd isotope following the equation ($\varepsilon Hf = 1.59\varepsilon Nd + 1.28$) given by Chauvel et al. (2008) because of the statistically significant Hf–Nd isotope ratio correlation (Zindler and Hart, 1986).

Appendix 1: The Sr-Nd-Hf isotopes replicate analyses results of the international reference materials

Sample	$^{87}Sr/^{86}Sr$	±2σ	$^{143}Nd/^{144}Nd$	±2σ	$^{176}Hf/^{177}Hf$	±2σ
JG-3	0.705372	0.000012	0.512627	0.000004	0.282743	0.000007
JG-3	0.705384	0.000008	0.512619	0.000004		
BHVO-2	0.703474	0.000012	0.512976	0.000006	0.283096	0.000004
JG-3	0.705392	0.000012	0.512627	0.000006		
JG-3	0.705385	0.000010	0.512618	0.000006	0.282755	0.000005